

RESEARCH ARTICLE

The novel membrane protein Hoka regulates septate junction organization and stem cell homeostasis in the *Drosophila* gut

Yasushi Izumi^{1,2,*}, Kyoko Furuse¹ and Mikio Furuse^{1,2}

ABSTRACT

Smooth septate junctions (sSJs) regulate the paracellular transport in the intestinal tract in arthropods. In *Drosophila*, the organization and physiological function of sSJs are regulated by at least three sSJ-specific membrane proteins: Ssk, Mesh and Tsp2A. Here, we report a novel sSJ membrane protein, Hoka, which has a single membrane-spanning segment with a short extracellular region, and a cytoplasmic region with Tyr-Thr-Pro-Ala motifs. The larval midgut in *hoka* mutants shows a defect in sSJ structure. Hoka forms a complex with Ssk, Mesh and Tsp2A, and is required for the correct localization of these proteins to sSJs. Knockdown of *hoka* in the adult midgut leads to intestinal barrier dysfunction and stem cell overproliferation. In *hoka*-knockdown midguts, aPKC is upregulated in the cytoplasm and the apical membrane of epithelial cells. The depletion of aPKC and *yki* in *hoka*-knockdown midguts results in reduced stem cell overproliferation. These findings indicate that Hoka cooperates with the sSJ proteins Ssk, Mesh and Tsp2A to organize sSJs, and is required for maintaining intestinal stem cell homeostasis through the regulation of aPKC and Yki activities in the *Drosophila* midgut.

KEY WORDS: *Drosophila*, Midgut, Smooth septate junction, Epithelial cell, Intestinal stem cells

INTRODUCTION

Epithelia separate distinct fluid compartments within the bodies of metazoans. For this epithelial function, occluding junctions act as barriers that control the free diffusion of solutes through the paracellular pathway. Septate junctions (SJs) are occluding junctions in invertebrates (Furuse and Tsukita, 2006; Lane et al., 1994; Tepass and Hartenstein, 1994) and form circumferential belts along the apicolateral region of epithelial cells. In transmission electron microscopy, SJs are observed between the parallel plasma membranes of adjacent cells, with ladder-like septa spanning the intermembrane space (Lane et al., 1994; Tepass and Hartenstein, 1994). Arthropods have two types of SJs: pleated SJs (pSJs) and smooth SJs (sSJs) (Banerjee et al., 2006; Lane et al., 1994; Tepass and Hartenstein, 1994; Jonusaite et al., 2016). pSJs are found in ectoderm-derived epithelia and surface glia surrounding the nerve cord, whereas sSJs are found mainly in the endoderm-derived epithelia, such as the midgut and gastric caeca (Lane et al., 1994; Tepass and Hartenstein, 1994). Despite being derived from the ectoderm, the outer epithelial layer of the proventriculus (OELP)

and the Malpighian tubules also possess sSJs (Lane et al., 1994; Tepass and Hartenstein, 1994). Furthermore, pSJs and sSJs are distinguished by the arrangement of septa. For example, the septa of pSJs form regular undulating rows, whereas those in sSJs form regularly spaced parallel lines in the oblique sections in lanthanum-treated preparations (Lane and Swales, 1982; Lane et al., 1994). To date, more than 20 pSJ-related proteins have been identified and characterized in *Drosophila* (Banerjee et al., 2006; Izumi and Furuse, 2014; Tepass et al., 2001; Wu and Beitel, 2004; Rouka et al., 2020). In contrast, only three membrane-spanning proteins, Ssk, Mesh and Tsp2A, have been reported as specific molecular constituents of sSJs (sSJ proteins) in *Drosophila* (Furuse and Izumi, 2017). Therefore, the mechanisms underlying sSJ organization and the functional properties of sSJs remain poorly understood compared with pSJs. Ssk has four membrane-spanning domains; two short extracellular loops, cytoplasmic N- and C-terminal domains, and a cytoplasmic loop (Yanagihashi et al., 2012). Mesh is a cell-cell adhesion molecule, which has a single-pass transmembrane domain and a large extracellular region containing a NIDO domain, an Ig-like E set domain, an AMOP domain, a vWD domain and a sushi domain (Izumi et al., 2012). Tsp2A is a member of the tetraspanin family of integral membrane proteins in metazoans with four transmembrane domains, N- and C-terminal short intracellular domains, two extracellular loops and one short intracellular turn (Izumi et al., 2016). The loss of *ssk*, *mesh* and *Tsp2A* causes defects in the ultrastructure of sSJs and the barrier function against a 10 kDa fluorescent tracer in the *Drosophila* larval midgut (Yanagihashi et al., 2012; Izumi et al., 2012, 2016). Ssk, Mesh and Tsp2A interact physically and are mutually dependent for their sSJ localization (Izumi et al., 2012, 2016). Thus, Ssk, Mesh and Tsp2A act together to regulate the formation and barrier function of sSJs. Furthermore, Ssk, Mesh and Tsp2A are localized in the epithelial cell-cell contact regions in the *Drosophila* Malpighian tubules in which sSJs are present (Tepass and Hartenstein, 1994; Yanagihashi et al., 2012; Izumi et al., 2012, 2016). Recent studies have shown that the knockdown of *mesh* and *Tsp2A* in the epithelium of Malpighian tubules leads to defects in epithelial morphogenesis, tubule transepithelial fluid and ion transport, and paracellular macromolecule permeability in the tubules (Jonusaite et al., 2020; Beyenbach et al., 2020). Thus, sSJ proteins are involved in the development and maintenance of functional Malpighian tubules in *Drosophila*.

The *Drosophila* adult midgut consists of a pseudostratified epithelium, which is composed of absorptive enterocytes (ECs), secretory enteroendocrine cells (EEs), intestinal stem cells (ISCs), EC progenitors (enteroblasts: EBs) and EE progenitors (enteroendocrine mother cells: EMCs) (Micchelli and Perrimon, 2006; Ohlstein and Spradling, 2006; Guo and Ohlstein, 2015). The sSJs are formed between adjacent ECs and between ECs and EEs (Resnik-Docampo et al., 2017). To maintain midgut homeostasis, ECs and EEs are continuously renewed by proliferation and

¹Division of Cell Structure, National Institute for Physiological Sciences, Okazaki 444-8787, Japan. ²Department of Physiological Sciences, The Graduate University of Advanced Studies, SOKENDAI, Okazaki 444-8585, Japan.

*Author for correspondence (yizumi@nips.ac.jp)

 Y.I., 0000-0001-6726-1246; M.F., 0000-0003-2847-8156

Handling Editor: Kathleen Green
Received 10 November 2020; Accepted 1 February 2021

differentiation of the ISC lineage through the production of intermediate differentiating cells, EBs and EMCs. Recently, we and other groups reported that the knockdown of sSJ proteins Ssk, Mesh and Tsp2A in the midgut causes intestinal hypertrophy accompanied by the overproliferation of ECs and ISC (Salazar et al., 2018; Xu et al., 2019; Izumi et al., 2019; Chen et al., 2020). These results indicate that sSJs play a crucial role in maintaining tissue homeostasis through the regulation of stem cell proliferation and enterocyte behavior in the *Drosophila* adult midgut. Furthermore, Chen et al. (2018) have reported that the loss of *mesh* and *Tsp2A* in adult midgut epithelial cells causes defects in cellular polarization, although no remarkable defects in epithelial polarity were found in the first-instar larval midgut cells of *ssk*, *mesh* and *Tsp2A* mutants (Yanagihashi et al., 2012; Izumi et al., 2012, 2016). Thus, sSJs may contribute to the establishment of epithelial polarity in the adult midgut.

During the regeneration of the *Drosophila* adult midgut epithelium, various signaling pathways are involved in the proliferation and differentiation of the ISC lineage (Jiang et al., 2016). Atypical protein kinase C (aPKC) is an evolutionarily conserved key determinant of apical-basal epithelial polarity (Ohno et al., 2015). Importantly, Chen et al. (2018) have reported that aPKC is dispensable for the establishment of epithelial cell polarity in the *Drosophila* adult midgut. Goulas et al. (2012) have reported that aPKC is required for differentiation of the ISC lineage in the midgut. The Hippo signaling pathway is involved in maintaining tissue homeostasis in various organs (Zheng and Pan, 2019). In the *Drosophila* midgut, inhibition of the Hippo signaling pathway activates the transcriptional co-activator Yorkie (Yki), which results in accelerated ISC proliferation via the Unpaired (Upd)-Jak-Stat signaling pathway (Karpowicz et al., 2010; Ren et al., 2010; Shaw et al., 2010). Recent studies have shown that Yki is involved in ISC overproliferation caused by the depletion of sSJ proteins in the midgut (Xu et al., 2019; Chen et al., 2020). Furthermore, Xu et al. (2019) have shown that aPKC is activated in the *Tsp2A*-RNAi-treated midgut, leading to activation of its downstream target Yki and causing ISC overproliferation through the activation of the Upd-Jak-Stat signaling pathway. Thus, crosstalk between aPKC and the Hippo signaling pathways appears to be involved in ISC overproliferation caused by *Tsp2A* depletion.

To further understand the molecular mechanisms underlying sSJ organization, we performed a deficiency screen for Mesh localization and identified the integral membrane protein Hoka as a novel component of *Drosophila* sSJs. Hoka consists of a short extracellular region and the characteristic repeating 4-amino acid motifs in the cytoplasmic region, and is required for the organization of sSJ structure in the midgut. Hoka and Ssk, Mesh, and Tsp2A show interdependent localization at sSJs and form a complex with each other. The knockdown of *hoka* in the adult midgut results in intestinal barrier dysfunction, aPKC- and Yki-dependent ISC overproliferation, and epithelial tumors. Thus, Hoka plays an important role in sSJ organization and in maintaining ISC homeostasis in the *Drosophila* midgut.

RESULTS

Hoka is involved in sSJ formation

We previously queried *Drosophila* strains that were defective in sSJ accumulation of Mesh using a genetic screen for a chromosomal deficient stock from the Bloomington Deficiency Kit. We found several deficiencies that caused an abrogated sSJ accumulation of Mesh in the stage 16 embryo OELP (Izumi et al., 2016). The *Tsp2A*

gene was identified as being responsible for Mesh localization in the screen (Izumi et al., 2016), and we found that the OELP of Df(3L)BSC371 (deleted segment: 64C1-64E1) showed cytoplasmic distribution of Mesh. To identify the precise genomic region responsible for the phenotype, we observed the Mesh distribution with other deficiencies overlapping with Df(3L)BSC371. The OELP of Df(3L)ED210 (deleted segment: 64B9-64C13) (Fig. 1A,B) and Df(3L)Exel6102 (deleted segment: 64B13-64C4) exhibited a cytoplasmic distribution phenotype for Mesh but not that of Df(3L)Exel6103 (deleted segment: 64C4-64C8), and the phenotype for Df(3L)BSC371 was mapped to the 64C1-64C4 interval. Within the genomic region 64C1-64C4, we focused on *CG13704* (Fig. 1C) as it was highly expressed in the midgut and Malpighian tubules (www.flybase.org/reports/FBgn0035583). *CG13704* encodes a putative single-pass transmembrane protein of 136 amino acids with a signal peptide and a transmembrane region (Fig. 1E), which is conserved in insects alone. We named the CG13704 protein 'Hoka' based on its immunostaining images in the midgut (see below; Hoka means honeycomb in Japanese). The mature Hoka protein appears to have a short N-terminal extracellular region (13 amino acids) after cleavage of the signal peptide (www.uniprot.org/uniprot/Q8XSX4). Interestingly, the C-terminal region is threonine-rich and includes three tyrosine-threonine-proline-alanine (YTPA) motifs. Multiple sequence alignment of Hoka using Multiple Alignment using Fast Fourier Transform (MAFFT) revealed that three types of Hoka homologs (three, two and single YTPA motif-containing homologs) are present in *Drosophila* (Fig. 1E; Fig. S1A). Other holometabolous insects have the same or similar motif: the mosquito and beetle homologs have a single YTPA motif; the butterfly, ant, bee, sawfly and moth homologs have a single YQPA motif; and the flea homolog has a single YTAA motif (Fig. S1B). In contrast, the motif is not present in the homologs of hemimetabolous insects, such as the psyllid, aphid, planthopper, miridae, termite and thrip.

To examine whether Hoka is associated with sSJs, we expressed C-terminally GFP-tagged Hoka (Hoka-GFP) in flies using *da-GAL4* (Fig. 1F–F", see below). In the stage 16 OELP, Hoka-GFP was detected in the apicolateral region with some cytoplasmic aggregates. Mesh colocalized with Hoka-GFP in the apicolateral region (Fig. 1F', F"), and therefore, we characterized Hoka as an sSJ-associated molecule.

To investigate whether Hoka is involved in sSJ formation, we generated *hoka* mutants using the CRISPR/Cas9 method provided by Fly Stocks of National Institute of Genetics (NIG-Fly; Kondo and Ueda, 2013). We obtained three independent *hoka* mutant strains (*hoka*^{x113}, *hoka*^{x127} and *hoka*^{x211}), all of which had small indel mutations encompassing the target site (Fig. 1D). These *hoka*-mutant embryos hatched into first-instar larvae but died at this stage (data not shown). All *hoka* mutants had frameshifts and premature stop codons. In the *hoka*^{x113}, *hoka*^{x127} and *hoka*^{x211} mutant stage 16 OELP, Mesh was diffusely distributed in the cytoplasm (Fig. S2F'–I"). Among these mutant strains, we mainly used the *hoka*^{x211} mutant for further experiments. To confirm that the lack of *hoka* caused cytoplasmic distribution of Mesh, we expressed Hoka-GFP in *hoka*-mutant flies using *da-GAL4*. The apicolateral accumulation of Mesh in the OELP was recovered and Hoka-GFP colocalized with Mesh in the Hoka-GFP-expressing *hoka* mutant OELP (Fig. 1I–I"), whereas Mesh remained in the cytoplasm of the control *hoka* mutant OELP without Hoka-GFP expression (Fig. 1G–H"). These observations indicate that Hoka is responsible for sSJ organization.

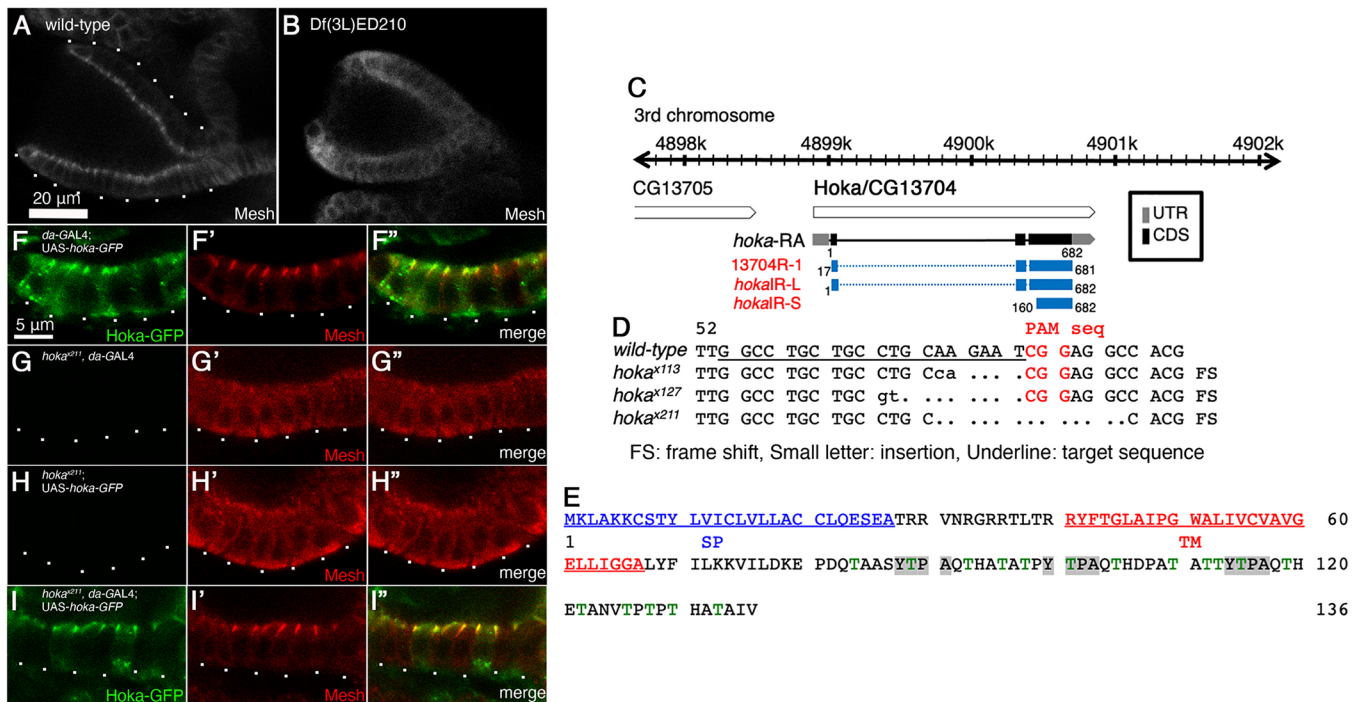


Fig. 1. Identification of *hoka* as an sSJ-related gene via a deficiency screen. (A,B) Immunofluorescence staining of embryonic stage 16 wild-type (A) and Df(3L)ED210 (B) OELPs using an anti-Mesh antibody. Basal membranes are delineated by dots (A). (C) Schematic of the *Drosophila* third-chromosome containing the *hoka* gene. Full-length genes of *hoka/CG13704* are contained in this region. The *hoka* DNA sequence used for the construction of *hoka*-RNAi (13704R-1, *hokalR*-L and *hokalR*-S) is indicated by blue lines. Gray bar represents the untranslated regions (UTR) of the *hoka* transcript/*hoka*-RA (mRNA isoform A). Black bar represents the coding sequences (CDS) of the *hoka* transcript/*hoka*-RA. (D) Genomic sequences of *hoka*-mutations induced by the CRISPR/Cas9 method. The nucleotide sequence of wild-type *hoka* from the start codon is shown at the top. The gRNA target sequence is underlined and the protospacer adjacent motif (PAM) sequence is shown in red. Deleted nucleotides are shown as dots. Inserted nucleotides are shown in lowercase letters. (E) Amino acid sequence of Hoka. The Hoka polypeptide contains a signal peptide (SP, blue), a transmembrane region (TM, red) and three Tyr-Thr-Pro-Ala repeat motifs (YTPA, highlighted in gray) in the threonine-rich (green) cytoplasmic region. (F-F'') Immunofluorescence staining of the Hoka-GFP-expressing stage 16 OELP (*da*-GAL4; UAS-*hoka*-GFP) using anti-GFP (F,F') and anti-Mesh (F',F'') antibodies. Hoka-GFP colocalizes with Mesh at sSJs. (G-I'') Immunofluorescence staining of *hoka*^{x211}-mutant (*hoka*^{x211}, *da*-GAL4, G-G'; *hoka*^{x211}, UAS-*hoka*-GFP, H-H') and Hoka-GFP-expressing *hoka*^{x211}-mutant (*hoka*^{x211}, *da*-GAL4, UAS-*hoka*-GFP, I-I'') stage 16 OELPs using anti-GFP (G,G',H,H',I,I') and anti-Mesh (G',G'',H'',H'',I'',I'') antibodies. Basal membranes are delineated by dots.

Hoka is a novel sSJ protein

To determine the expression pattern and the subcellular localization of endogenous Hoka, we used two anti-Hoka antibodies that were raised against the C-terminal cytoplasmic region of Hoka. In a western blot analysis, the anti-Hoka antibodies detected an intense ~21 kDa band in the extracts from whole wild-type first-instar larvae (Fig. S2A). The ~21 kDa band was absent in *hoka* mutant extracts (Fig. S2A), indicating that the ~21 kDa band represents Hoka. Immunofluorescence microscopy analyses revealed that an anti-Hoka antibody (29-1) labeled the midgut and the apicolateral region of the OELP in late-stage embryos (Fig. 2A,A'; Fig. S2F). The staining pattern of the OELP with the antibody overlapped that of the anti-Mesh antibody (Fig. 2A'; Fig. S2F-F''). Furthermore, the immunoreactivity of the antibody in the OELP and midgut was reduced in the *hoka* mutant embryos (Fig. S2G-I), demonstrating the specificity of the anti-Hoka antibody. Immunofluorescence staining of the first-instar larvae revealed honeycomb-like signals for Hoka in the midgut, OELP and Malpighian tubules, but not in the foregut and hindgut (Fig. 2B,C). At a higher magnification, staining with the anti-Hoka antibody overlapped with that of the anti-Mesh antibody in the apicolateral region of the midgut epithelial cells (Fig. 2E-E''). The anti-Hoka antibody also labeled the cell-cell contacts in adult midgut epithelial cells (Fig. 2D) and coincided with the staining of the anti-Mesh antibody in the apicolateral region (Fig. 2F-F''). Taken together, these observations

indicate that Hoka is a component of sSJs in *Drosophila* from the embryo to adulthood.

We next investigated whether the localization of Hoka is affected by the loss of Mesh, Ssk or Tsp2A. In the Df(3L)ssk, *mesh*⁰⁴⁹⁵⁵ and *Tsp2A*¹⁻² mutant first-instar larval midgut epithelial cells, Hoka failed to localize to the apicolateral region but was distributed diffusely and formed aggregates in the cytoplasm (Fig. 2G,G',H, H'',I,I',J,J''), although Dlg (also known as Dlg1) was present in the apicolateral region (Fig. 2G',G'',H'',H'',I'',I'',J'',J''). Thus, Ssk, Mesh and Tsp2A are required for the sSJ localization of Hoka.

Hoka is required for the initial assembly of sSJ proteins

We next examined Hoka distribution during sSJ formation using immunofluorescence staining of wild-type embryos from stage 14 to stage 16. In the OELP of stage 14 embryos, Hoka was distributed in the cytoplasm and along the lateral membranes (Fig. S3A), and was localized along the lateral membrane with partial accumulation in the apicolateral region in the stage 15 OELP (Fig. S3B). In the stage 16 OELP, Hoka accumulated at the apicolateral region (Fig. S3C), suggesting that it is incorporated into the sSJs during stage 15 to stage 16 of embryonic development. These signals are specific for Hoka, as they were absent in the *hoka* mutant (Fig. S3D-F). Notably, the sSJ targeting property of Hoka was similar to that of Mesh during sSJ formation of OELP (Fig. S3A'-C'').

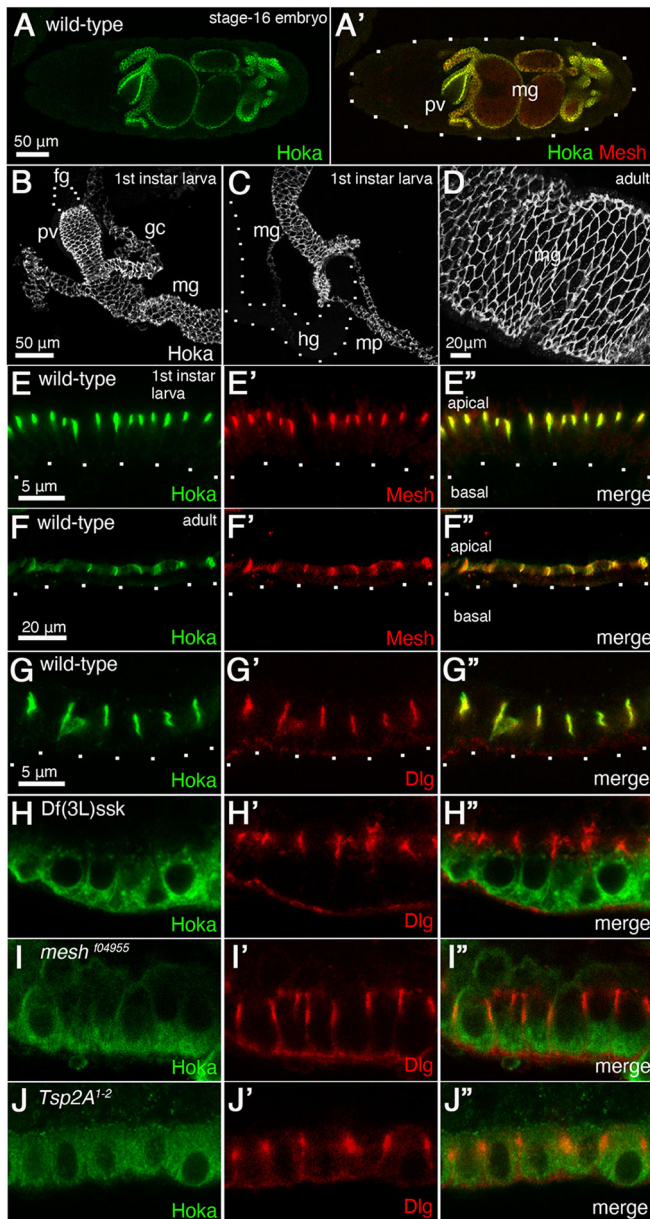


Fig. 2. Hoka localizes to sSJs. (A,A') Immunofluorescence staining of a stage 16 wild-type embryo using anti-Hoka (A,A') and anti-Mesh (A') antibodies. The outline of the embryo is delineated by dots. (B–D) Immunofluorescence staining of the wild-type first-instar larval anterior midgut (B), posterior midgut (C) and adult midgut (D) using an anti-Hoka antibody. Hoka is expressed in the first-instar larval midgut, the OELP and the Malpighian tubules (B,C). Hoka signals were not detected in the foregut (B) or hindgut (C). (E–F'') Immunofluorescence staining of the wild-type first-instar larval (E–E'') and adult (F–F'') midgut using anti-Hoka (green in E,F) and anti-Mesh (red in E',F') antibodies. Basal membranes are delineated by dots. (G–J'') The first-instar larval midgut of wild-type, *Df(3 L)ssk*, *mesh*¹⁰⁴⁹⁵⁵-mutant and *Tsp2A*¹⁻²-mutant stained with anti-Hoka (green in G–J) and anti-Dlg (red in G'–J') antibodies. fg, foregut; gc, gastric caeca; hg, hindgut; mg, midgut; mp, Malpighian tubules; pv, proventriculus.

To test whether the *hoka*-mutation affects the initial assembly of sSJ proteins, we monitored the distribution of Ssk, Mesh and Tsp2A during sSJ maturation in the OELP of wild-type and *hoka* mutant embryos. In the wild-type OELP, a faint apicolateral distribution of Ssk, Mesh and Tsp2A was observed at stage 15 (Fig. S3B',H,N), and they were detectable in the apicolateral region at stage 16

(Fig. S3C',I,O). By contrast, in the *hoka* mutant OELP, Ssk, Mesh and Tsp2A failed to accumulate in the apicolateral region during stage 15 to stage 16 of development (Fig. S3E'–E'',F'–F'',K,L,Q,R). Together, these results indicate that Hoka is required for the initial assembly of sSJ proteins in the OELP.

Hoka is required for efficient localization of sSJ proteins to the apicolateral region

We next observed the distribution of sSJ proteins in the *hoka* mutant larval OELP and midgut. As reported previously, Dlg, Ssk, Mesh and Tsp2A are present in sSJs in the wild-type first-instar larval OELP and midgut (Yanagihashi et al., 2012; Izumi et al., 2012, 2016) (Fig. 3A',C–E,I,K–M). Interestingly, in the *hoka* mutant first-instar larval OELP, Ssk was distributed in the apical and apicolateral region (Fig. 3F), and Mesh and Tsp2A were present in the apicolateral region (Fig. 3G,H). Dlg was localized at the apicolateral region (Fig. 3B'). These data are in contrast to the observation that Mesh and Tsp2A were distributed diffusely in the cytoplasm, and Ssk was mislocalized to the apical and the lateral membranes in the *hoka* mutant stage 16 OELP (Fig. S3F',L,R). In the *hoka* mutant first-instar larval midgut epithelial cells, Ssk was mislocalized to the apical and lateral membrane (Fig. 3N), and Mesh and Tsp2A were mislocalized along the lateral membrane (Fig. 3O,P). We occasionally observed the apicolateral accumulation of Ssk, Mesh and Tsp2A in the mutant midgut epithelial cells (Fig. 3Q–S). Dlg was localized in the apicolateral region (Fig. 3J'). Taken together, these results indicate that Hoka is required for the efficient localization of Ssk, Mesh and Tsp2A to the apicolateral region in epithelial cells.

Western blot analyses revealed that the densities of the main bands of Ssk (~15 kDa) and Tsp2A (~21 kDa) were not significantly changed in *hoka* mutant larvae, compared with wild-type larvae (Fig. S2B,C). However, the density of Mesh at ~200 kDa and ~90 kDa in the *hoka* mutant appeared to be increased compared to the wild-type (Fig. S2E), suggesting that Hoka may be involved in the regulation of Mesh protein levels.

Hoka is required for the proper organization of the sSJ structure

To investigate the role of Hoka in the organization of the sSJ structure, the ultrastructure of the *hoka* mutant first-instar larval midgut was examined by electron microscopy. In the wild-type midgut, sSJs were observed as parallel plasma membranes with ladder-like septa in the apicolateral region of bicellular contacts (Fig. 4A,B). In the *hoka* mutant midgut, proper sSJ structures were barely detectable at the apicolateral region of bicellular contacts (Fig. 4C–H), although ladder-like structures were occasionally visible (Fig. 4C–E, brackets). Large gaps were often formed between the apicolateral membranes of adjacent cells (Fig. 4F–H, asterisks). Thus, sSJs fail to form correctly in the *hoka* mutant midgut, although Ssk, Mesh and Tsp2A are present in the lateral regions (Fig. 3N–S). These results indicate that Hoka is required for the proper organization of sSJ structure.

Hoka forms a complex with Ssk, Mesh and Tsp2A

As Ssk, Mesh and Tsp2A form a complex *in vivo* (Izumi et al., 2012, 2016), we examined whether Hoka is physically associated with Ssk, Mesh and Tsp2A. *Drosophila* embryonic extracts were immunoprecipitated using anti-Hoka antibodies, and endogenous Ssk and Mesh were co-precipitated with Hoka (Fig. 5A). Additionally, Hoka was co-immunoprecipitated with Ssk and Mesh from embryonic extracts with anti-Ssk and anti-Mesh

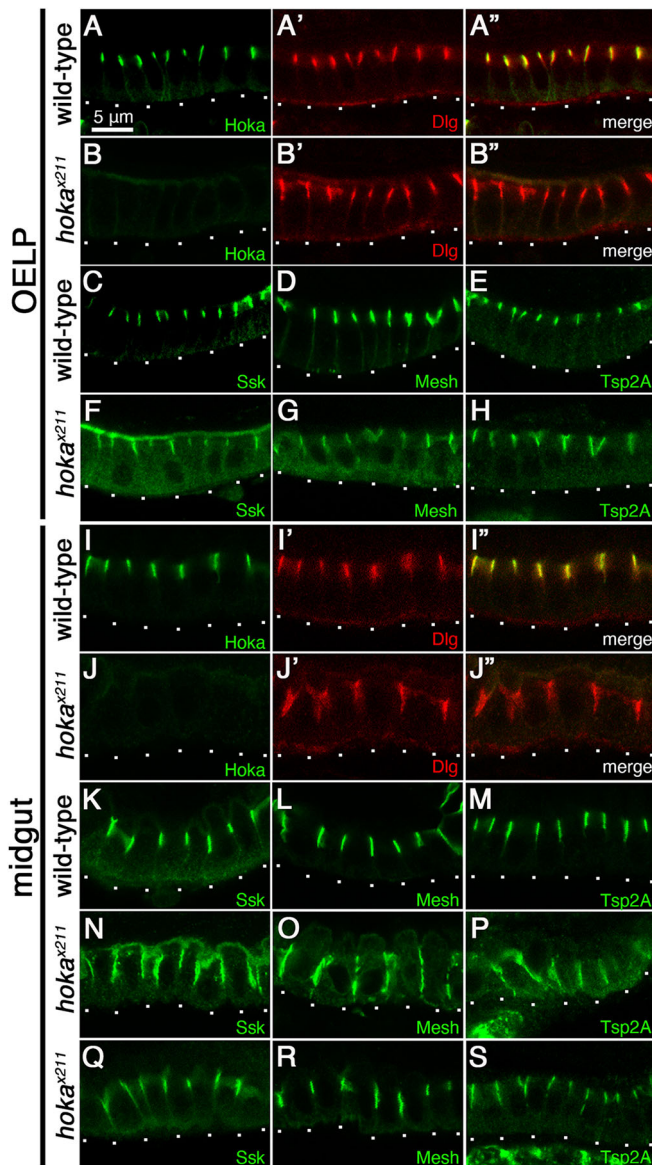


Fig. 3. Hoka is required for the localization of sSJ proteins. (A–B'') The first-instar larval OELPs of wild-type (A–A'') and *hoka*^{x211}-mutants (B–B'') stained with anti-Hoka (green in A,A'',B,B'') and anti-Dlg (red in A',A'',B',B'') antibodies. (C–H) The first-instar larval OELPs of wild-type (C–E) and *hoka*^{x211}-mutant (F–H) stained with anti-Ssk (C,F), anti-Mesh (D,G) and anti-Tsp2A (E,H) antibodies. (I–J'') The first-instar larval midgut of wild-type (I–I'') and *hoka*^{x211}-mutant (J–J'') stained with anti-Hoka (green in I,I'',J,J'') and anti-Dlg (red in I',I'',J',J'') antibodies. (K–S) The first-instar larval midgut of wild-type (K–M) and *hoka*^{x211}-mutant (N–S) stained with anti-Ssk (K,N,Q), anti-Mesh (L,O,R) and anti-Tsp2A (M,P,S) antibodies. Basal membranes are delineated by dots.

antibodies, respectively (Fig. 5B). Neither Hoka, Mesh nor Ssk was precipitated by the pre-immune sera or the control IgG (Fig. 5A,B). Embryos expressing enhanced GFP (EGFP)-Tsp2A with the *daughterless* (*da*)-GAL4 driver were subjected to immunoprecipitation with anti-GFP antibodies, and EGFP-Tsp2A was found to co-precipitate with endogenous Hoka (Fig. 5C). Hoka was not precipitated from EGFP-Tsp2A-expressing embryos with the control IgG, or EGFP-expressing embryos with the anti-GFP antibody (Fig. 5C). These results indicate that Hoka forms a complex with Ssk, Mesh and Tsp2A *in vivo*.

Knockdown of *hoka* in the adult ECs leads to increased stem cell proliferation

Recently, we and other groups reported that the knockdown of *ssk*, *mesh* or *Tsp2A* in adult ECs led to a remarkably shortened lifespan in adult flies, increased ISC proliferation and intestinal hypertrophy, accompanied by the accumulation of ECs in the midgut (Salazar et al., 2018; Xu et al., 2019; Izumi et al., 2019; Chen et al., 2020). Therefore, we investigated whether the knockdown of *hoka* from adult ECs also caused similar phenotypes to knockdowns of other sSJ proteins. To knockdown *hoka* in the adult midgut, inducible *hoka*-RNAi was performed using the Gal4/UAS system with an EC-specific driver *Myo1A*-GAL4 and the temperature-sensitive (ts) GAL4 repressor, *tubGal80^{ts}* (McGuire et al., 2004; Jiang et al., 2009). *Myo1A*-Gal4 *tubGal80^{ts}*, UAS-*Luciferase* (*Luc*)-RNAi (control), or UAS-*hoka*-RNAi (13704R-1, *hoka*IR-L or *hoka*IR-S; Fig. 1C), flies were raised to adults at 18°C (permissive temperature) and then shifted to 29°C (non-permissive temperature) to inactivate GAL80, leading to the activation of the GAL4/UAS system to express each UAS-driven transgene. Western blot analysis of lysates from the control and the *hoka*-RNAi midgut showed that the Hoka protein level was decreased in the *hoka*-RNAi midgut, compared to the control midgut (Fig. 6A). In the *hoka*-RNAi midgut, Ssk, Mesh, Tsp2A and Dlg were still observed in the lateral membrane of the ECs (Fig. S4). This was consistent with the observation that Ssk, Mesh and Tsp2A were distributed to the lateral or apicolateral region in the *hoka* mutant larval midgut (Fig. 3N–S). Adult flies expressing *hoka*-RNAi had a shortened lifespan compared to the control flies (Fig. 6B). We also examined whether the barrier function of the midgut was disrupted in *hoka*-RNAi flies. According to the method for a Smurf assay (Rera et al., 2011, 2012), flies were fed a non-absorbable 800-Da blue food dye in sucrose solution. At 5 days after transgene induction, the knockdown of *hoka* in ECs led to a significant increase in flies with blue dye throughout their body cavity, indicating a dysfunction in the midgut barrier (Fig. 6D). The extent of midgut barrier dysfunction in the flies further increased at 8 days after transgene induction, compared with age-matched controls (Fig. 6C,D). Thus, Hoka contributes to the epithelial barrier function in the adult midgut.

Next, we examined whether ISC proliferation was increased in the *hoka*-RNAi midgut. Staining the midgut with the phospho-histone H3 (PH3) antibody for the mitotic marker, we found that PH3⁺ cells were markedly increased in the *hoka*-RNAi midgut compared with the midgut in controls (Fig. 7A–C,J). Immunostaining of the midgut with an antibody against Delta, an ISC marker (Ohlstein and Spradling, 2006), showed that ISCs were increased in the *hoka*-RNAi midgut, compared with the midgut in controls (Fig. 7A–C). We also confirmed that the PH3⁺ cells were Delta⁺ (Fig. 7B,C). The expression of an additional RNAi line for *hoka* (*hoka*IR-S) in ECs also caused increased ISC proliferation (Fig. 7J). These results indicate that knockdown of *hoka* in ECs leads to increased ISC proliferation.

During the adult midgut epithelial regeneration, the Ras-MAP kinase and the Jak-Stat signaling pathways are involved in increased ISC proliferation (Beebe et al., 2010; Buchon et al., 2010; Karpowicz et al., 2010; Shaw et al., 2010; Biteau and Jasper, 2011; Jiang et al., 2009, 2011; Osman et al., 2012; Zhou et al., 2013). These pathways are activated in the *ssk*, *mesh* and *Tsp2A*-deficient midgut (Izumi et al., 2019). Therefore, we observed whether these signaling pathways were activated in the *hoka*-RNAi midgut. To monitor the Ras-MAP kinase pathway activity, we examined the levels of diphosphorylated ERK (dpERK) (Gabay

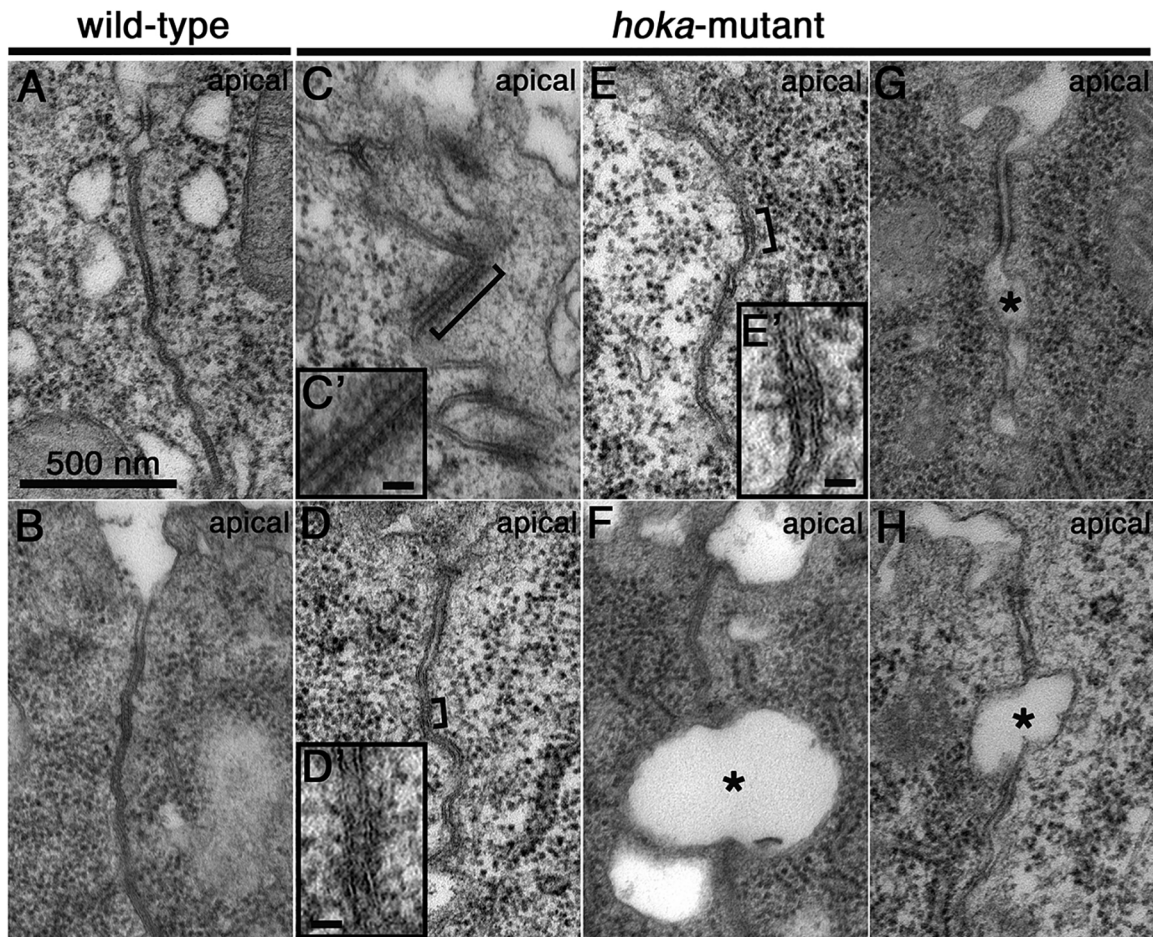


Fig. 4. Hoka is required for the correct organization of sSJ structure. (A–H) Transmission electron microscopy of the first-instar larval midgut in wild-type (A,B) and *hoka* mutants (C–H). In the wild-type midgut, typical sSJs are observed at bicellular contacts (A,B). In the *hoka* mutant midgut, proper sSJ structures are barely detectable at the apicolateral region of bicellular contact (C–H), although the ladder-like structures are occasionally visible (C–E, brackets). Large gaps are often formed between the apicolateral regions of adjacent cells (F–H, asterisks). Magnified views of the regions marked by brackets are shown in C', D' and E'. Scale bars: 500 nm (A–H); 200 nm (C'); 300 nm (D',E').

et al., 1997). In control flies, dpERK signals were barely detectable in the midgut (Fig. 7D). In contrast, intense dpERK signals were found in the *hoka*-RNAi midgut (Fig. 7E,F), indicating that the Ras-MAP kinase pathway was activated in ISCs. To monitor the Jak-Stat pathway activity, we used a Stat92E reporter line to drive the expression of the destabilized green fluorescent protein (DGFP) (10xSTAT-DGFP). In the control midgut, a few DGFP⁺ cells were observed (Fig. 7G), whereas DGFP⁺ cells were markedly increased in the *hoka*-RNAi midgut (Fig. 7H,I). Collectively, these results demonstrate that the knockdown of *hoka* in ECs results in the activation of both the Ras-MAP kinase and the Jak-Stat signaling pathways in the midgut.

We next evaluated the organization of the *hoka*-RNAi midgut epithelium. At 10 days after transgene induction, a simple epithelium in which ECs expressed CD8-GFP driven by *Myo1A*-Gal4 was observed in the control midgut (Fig. 7K). The organization of the epithelium was disrupted in the *hoka*-RNAi midgut, with several ECs accumulating in the posterior midgut lumen (Fig. 7L,M). In the posterior part of the midgut, the diameter was significantly expanded compared to the control midgut (Fig. 7Q). The ECs exhibited a variety of aberrant appearances, implying a polarity defect (Fig. 7N–P''). Aberrant distribution of the apical membrane marker phospho-Ezrin/Radixin/Moesin (pERM)

(Chen et al., 2018) and Dlg, a marker for the apicolateral membrane, was observed in the *hoka*-RNAi ECs (Fig. 7O–P''). Thus, knockdown of *hoka* in ECs causes intestinal tumor accompanied by the accumulation of ECs in the midgut lumen, indicating that Hoka is required for maintaining intestinal homeostasis in the adult fly. We performed *hoka*-RNAi in ISCs/EBs using an *escargot*^{ts} (*esg*^{ts})-GAL4 driver and observed increased ISC proliferation and accumulation of ECs in the midgut (Fig. S5), suggesting that Hoka function is required for ISC and/or EBs to regulate ISC behavior in the adult midgut.

aPKC and Yki are involved in ISC overproliferation caused by *hoka*-RNAi

In a recent study, the reduced expression of aPKC and the Hippo transcriptional co-activator Yki in *Tsp2A*-RNAi ISCs/EBs or ECs led to the reduction of *Tsp2A*-RNAi-induced ISC overproliferation in the midgut (Xu et al., 2019). The same study also showed that the expression of *Tsp2A*-RNAi in the midgut increases aPKC staining in the cell border membrane. We examined whether aPKC staining was increased in the *Myo1A*^{ts}-GAL4-driven *hoka*-RNAi midgut. In the control midgut, aPKC staining was barely detectable, but the signal intensity of aPKC staining was significantly increased in the *hoka*-RNAi midgut compared to the control midgut (Fig. 8A–C).

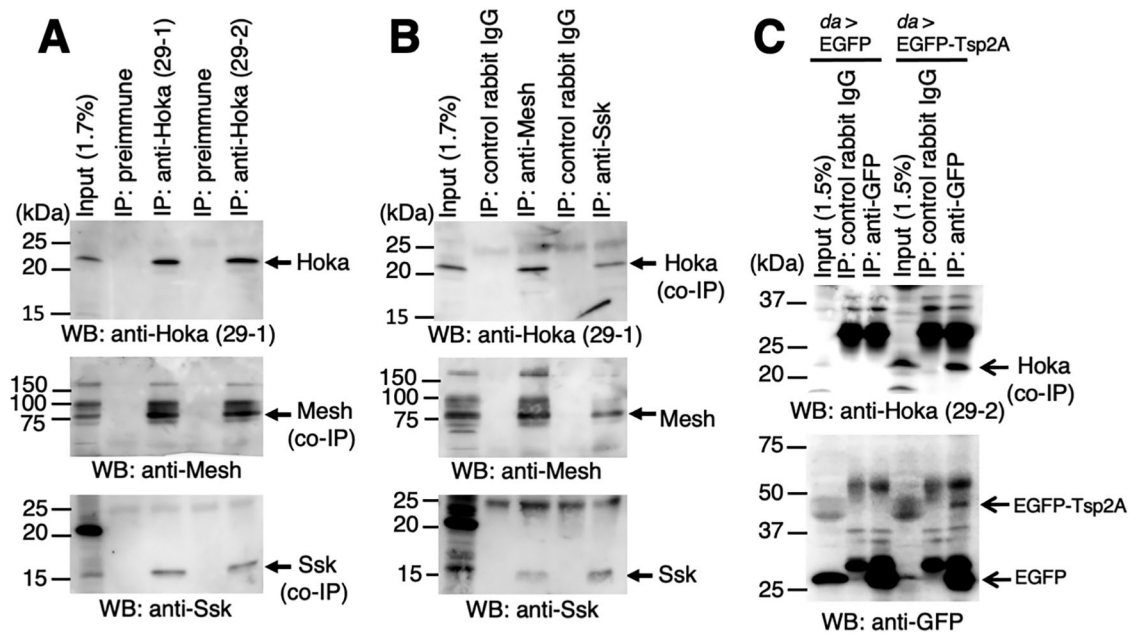


Fig. 5. Hoka forms a complex with Ssk, Mesh and Tsp2A. (A,B) Hoka co-immunoprecipitates with Ssk and Mesh. The embryonic extracts (Input) were subjected to immunoprecipitation (IP) with anti-Hoka (A), anti-Mesh (B) and anti-Ssk (B) antibodies. The immunocomplexes were separated on a 15% SDS-polyacrylamide gel, and western blot analyses were performed using anti-Hoka (upper panel), anti-Mesh (middle panel) and anti-Ssk (lower panel) antibodies. Hoka was immunoprecipitated with anti-Hoka antibodies, but not with the pre-immune serum (A, upper panel). The immunoprecipitates of Hoka contained Mesh (A, middle panel) and Ssk (A, lower panel). Mesh was immunoprecipitated with an anti-Mesh antibody, but not with a control IgG (B, middle panel). The immunoprecipitates of Mesh contained Hoka (B, upper panel) and Ssk (B, lower panel). Ssk was immunoprecipitated with an anti-Ssk antibody, but not with a control IgG (B, middle panel). The immunoprecipitates of Ssk contained Hoka (B, upper panel) and Mesh (B, lower panel). (C) Hoka co-immunoprecipitates with EGFP-Tsp2A. Extracts of embryos expressing *da-GAL4/EGFP* or *da-GAL4/EGFP-Tsp2A* (Input) were immunoprecipitated with an anti-GFP antibody. The immunocomplexes were separated on a 15% SDS-polyacrylamide gel, and western blot analyses were performed using anti-Hoka (upper panel) or anti-GFP (lower panel) antibodies. Immunoprecipitates of EGFP-Tsp2A (~50 kDa, arrow) with an anti-GFP antibody are shown (lower panel). EGFP was immunoprecipitated with an anti-GFP antibody from the embryos that expressed EGFP (arrow in lower panel). Hoka was co-precipitated with EGFP-Tsp2A but not with EGFP (arrow in upper panel). Hoka was not precipitated with a control IgG from embryos expressing EGFP-Tsp2A. The kDa indicated to the left of the images (A–C) refer to the marker band positions.

In the longitudinal cross-sections of the control midgut, apical membrane aPKC staining was occasionally observed in cells with a small nucleus (presumably ISCs) (Fig. 8D–D'', G–G'', arrowhead). aPKC has been reported to localize asymmetrically in the apical membrane of ISCs and regulates the differentiation of ISCs to EBs (Goulas et al., 2012). Interestingly, in the *hoka*-RNAi midgut, apical membrane staining of aPKC was often found in the cells mounted by other cells (Fig. 8E–E'', F–F'', H–H'', arrow). There are large and small nuclei-containing cells in the apical aPKC-localizing cells (Fig. 8E–E'', F–F'', H–H''). The apical aPKC staining partially overlapped with F-actin staining (Fig. 8E'', F'') and Dlg staining (Fig. 8H''). To clarify the cell types in which apical aPKC was observed, we expressed CD8-GFP together with *hoka*-RNAi using the *Myo1A^{ts}*-GAL4 in the midgut and stained the midgut with an anti-Delta antibody. Here, GFP⁺ and Delta⁺ cells were identified as ECs and ISCs, respectively. In the control midgut, apical aPKC staining was observed in the Delta⁺ ISCs (Fig. 8I–I''). In the *hoka*-RNAi midgut, three types of apical aPKC-localizing cells were observed (Fig. 8J–J'', K–K''): the Delta⁺ ISCs (arrowheads), the Delta⁻ and CD8-GFP⁻ cells (presumably EBs and/or EEs, arrows), and the Delta⁻ and CD8-GFP⁺ cells (EC-like cells, yellow arrows). These results indicate that aPKC can be apically localized in ISCs and the differentiated cells in the *hoka*-RNAi midgut.

Next, we investigated whether the depletion of *aPKC* and *yki* from *hoka*-RNAi ECs results in a reduction in ISC overproliferation caused by *hoka*-RNAi. To deplete the expression of *aPKC* and *yki* in *hoka*-RNAi ECs, we used *aPKC* (HMS01411) and *yki* (JF03119)

RNAi lines, both of which efficiently reduced ISC overproliferation caused by the *Tsp2A*-RNAi (Xu et al., 2019). Expression of *aPKC*-RNAi driven by *Myo1A^{ts}*-GAL4 in ECs did not lead to a significant difference in ISC proliferation, whereas expression of *yki*-RNAi moderately increased the proliferation compared to the control *Luc*-RNAi midgut (Fig. 8L). Expression of *hoka*-RNAi, together with *aPKC*-RNAi or *yki*-RNAi in ECs, significantly reduced ISC overproliferation compared to the *hoka*-RNAi and the *Luc*-RNAi midgut (Fig. 8L; Fig. S6A–D). Accumulation of cells in the midgut lumen was still observed in the *hoka*-RNAi, together with *aPKC*-RNAi or *yki*-RNAi midguts (Fig. S6E–H), probably due to the high rate of ISC proliferation in these midguts (Fig. 8L). Taken together, these results indicate that aPKC and Yki activities mediate ISC overproliferation caused by *hoka*-RNAi in the ECs.

DISCUSSION

The identification of Ssk, Mesh and Tsp2A has provided an experimental system to analyze the role of sSJs in the *Drosophila* midgut (Furuse and Izumi, 2017). Recent studies have shown that sSJs regulate the epithelial barrier function and also ISC proliferation and EC behavior in the midgut (Salazar et al., 2018; Xu et al., 2019; Izumi et al., 2019; Chen et al., 2020). Furthermore, sSJs are involved in epithelial morphogenesis, fluid transport and macromolecule permeability in the Malpighian tubules (Jonusaite et al., 2020; Beyenbach et al., 2020). Here, we have reported the identification of a novel sSJ-associated membrane protein Hoka. Hoka is required for the efficient accumulation of other sSJ proteins

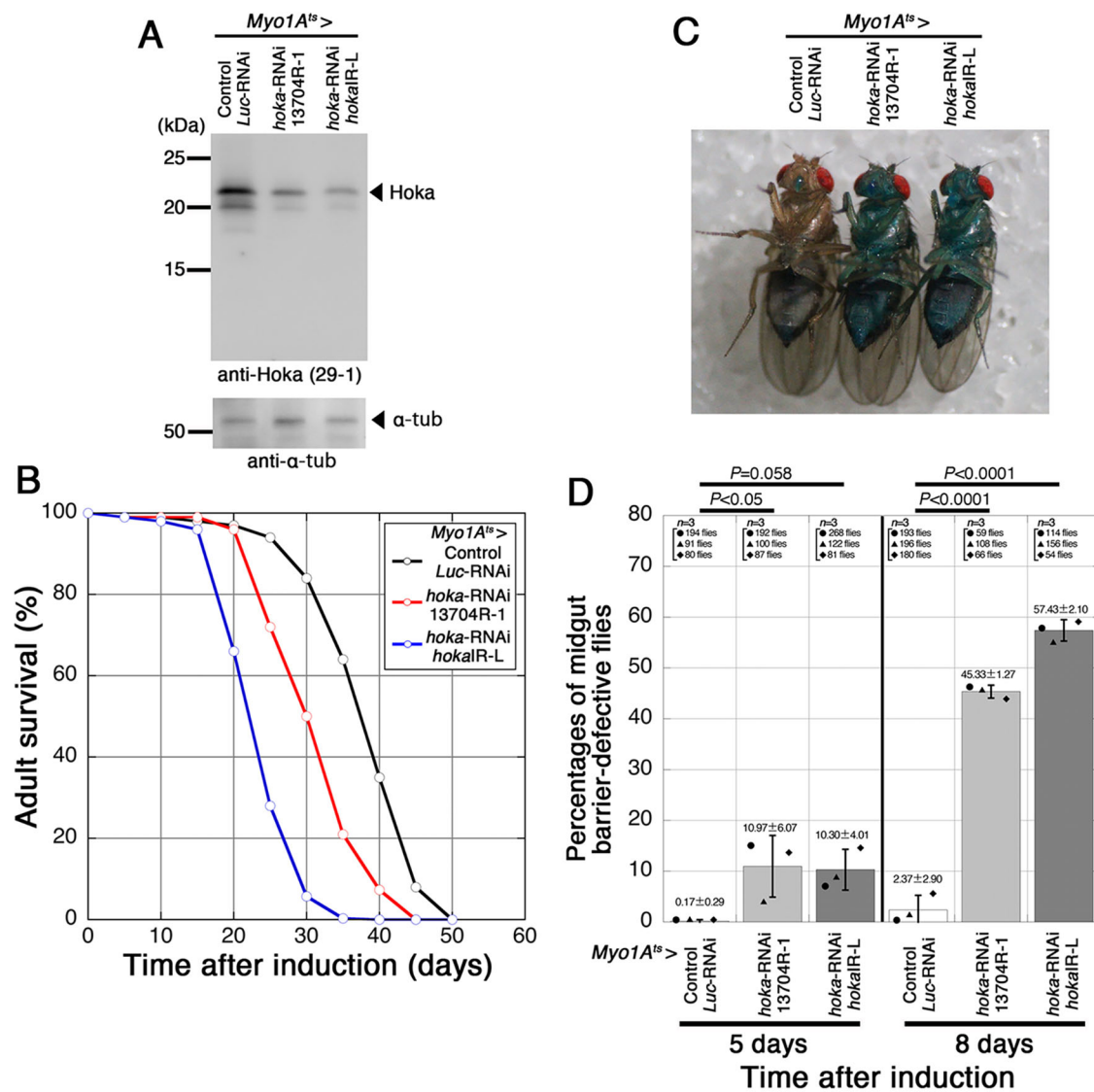


Fig. 6. Depletion of *hoka* from ECs in adult flies results in a shortened lifespan and midgut barrier dysfunction. (A) Western blot analyses of the *hoka*-RNAi adult midgut. Extracts of the adult midgut prepared from control (*Myo1A^{ts}*-Gal4/UAS-*Luc*-RNAi) or *hoka*-RNAi (*Myo1A^{ts}*-Gal4/UAS-*hoka*-RNAi 13704R-1 or *hokalR*-L) flies at 10 days after induction were separated on a 15% SDS-polyacrylamide gel, and western blot analyses were performed using the anti-Hoka (29-1, upper panel) and anti- α -tubulin (lower panel) antibodies. (B) Survival analysis of flies expressing *Myo1A^{ts}*-Gal4 with UAS-*Luc*-RNAi (control, $n=300$), UAS-*hoka*-RNAi 13704R-1 ($n=300$) or UAS-*hoka*-RNAi *hokalR*-L (15074R-1) ($n=300$). The transgenes were expressed with GAL80^{ts}; therefore, the flies were raised at 18°C until adulthood and were then moved to 29°C. Each vial contained 30 flies (15 females and 15 males). Median lifespan: *Luc*-RNAi, 37 days; *hoka*-RNAi 13704R-1, 30 days; and *hokalR*-L, 22 days. (C,D) Barrier integrity (Smurf) assays. Flies expressing *Myo1A^{ts}*-Gal4 with UAS-*Luc*-RNAi (control), UAS-*hoka*-RNAi 13704R-1 or UAS-*hoka*-RNAi *hokalR*-L were fed blue dye in sucrose solution. (C) A control fly and midgut barrier-defective *hoka*-deficient flies with blue bodies at 8 days after transgene induction. (D) Left to right: control ($n=3$; 194, 91 and 80 flies for each assay); *hoka*-RNAi 13704R-1 ($n=3$; 192, 100 and 87 flies); and *hoka*-RNAi *hokalR*-L ($n=3$; 268, 122 and 81 flies) at 5 days after induction; and control ($n=3$; 193, 196 and 180 flies); *hoka*-RNAi 13704R-1 ($n=3$; 59, 108 and 66 flies); and *hoka*-RNAi *hokalR*-L ($n=3$; 114, 156, and 54 flies) at 8 days after induction. The loss of midgut barrier function was determined when the dye was observed outside the midgut. Flies with blue color throughout the body were judged midgut barrier-defective flies, although the tone of the color varied depending on the affected flies. *hoka*-RNAi flies showed a loss of barrier function compared with control flies. Data are mean \pm s.e.m. from three independent assays. The dot plots represent the percentage of midgut barrier-defective flies in each assay. The numbers on the bar graphs represent the mean percentage of midgut barrier-defective flies (mean \pm s.e.m.). Statistical significance ($P < 0.05$, $P < 0.0001$) was evaluated using one-way ANOVA/Tukey's multiple comparisons tests.

at sSJs and the correct organization of sSJ structure. The knockdown of *hoka* in the adult midgut leads to intestinal barrier dysfunction, increased ISC proliferation mediated by aPKC and Yki activities, and epithelial tumors. Thus, Hoka contributes to sSJ organization and the maintenance of ISC homeostasis in the *Drosophila* midgut.

The unique primary structure of Hoka homolog proteins

Arthropod sSJs have been classified together based on their morphological similarity (Green and Bergquist, 1982; Lane et al.,

1994). The identification of sSJ proteins in *Drosophila* has provided an opportunity to investigate whether sSJs in various arthropod species share similarities at the molecular level. However, Hoka homolog proteins appear to be conserved only in insects upon a database search (data not shown), suggesting compositional variations in arthropod sSJs.

Interestingly, the cytoplasmic region of Hoka includes three YTPA motifs. The same or similar amino acid motifs are also present in the Hoka homologs of other holometabolous insects, such

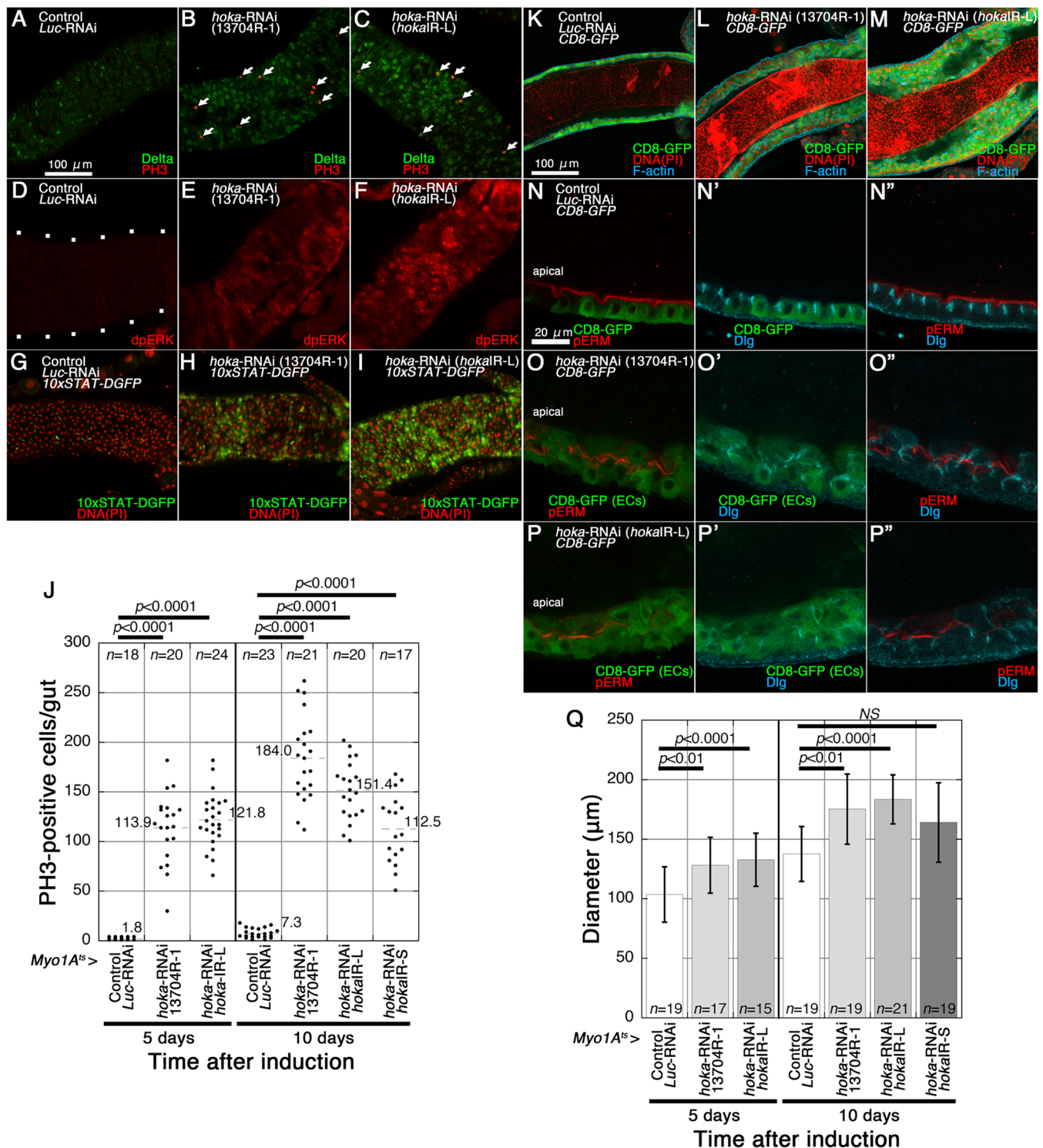


Fig. 7. See next page for legend.

as other *Drosophila* species, the mosquito, beetle (YTPA motif), butterfly, ant, bee, sawfly, moth (YQPA motif) and flea (YTAA motif), although the number of these motif(s) vary (1 to 3 in *Drosophila* species, 1 in other holometabolous insects). In contrast, the motif is not present in hemimetabolous insects. The extensive conservation of the YTPA/YQPA/YTAA motif in holometabolous insects suggests that the motif was evolutionarily acquired and plays a critical role in the molecular function of Hoka. It would be

interesting to investigate the role of the YTPA/YQPA/YTAA motif in sSJ organization of holometabolous insects.

The extracellular region of Hoka appears to be composed of 13 amino acids alone after the cleavage of the signal peptide, which is too short to bridge the 15–20 nm intercellular space of sSJs (Lane et al., 1994; Tepass and Hartenstein, 1994). Thus, Hoka is unlikely to act as a cell adhesion molecule in sSJs. Indeed, the overexpression of Hoka-GFP in *Drosophila* S2 cells did not

Fig. 7. The depletion of *hoka* from ECs leads to increased ISC proliferation and the accumulation of ECs in the adult midgut.

(A–C) Confocal images of the adult posterior midgut expressing *Myo1A^{ts}-Gal4* with UAS-*Luc-RNAi* (control, A), UAS-*hoka-RNAi* 13704R-1 (B) or UAS-*hoka-RNAi hokalR-L* (C) at 10 days after induction, and stained for PH3 (red, arrows) and Delta (green). (D–F) Confocal images of the adult posterior midgut expressing *Myo1A^{ts}-Gal4* with UAS-*Luc-RNAi* (control, D), UAS-*hoka-RNAi* 13704R-1 (E) or UAS-*hoka-RNAi hokalR-L* (F) at 10 days after induction, and stained for dpERK (red). The enhancement of Ras-MAPK pathway activity in the *hoka-RNAi* midgut is shown by the increased expression of dpERK (E,F). The outline of the midgut is delineated by dots (D). (G–I) Confocal images of the adult posterior midgut expressing *Myo1A^{ts}-Gal4/10xSTAT-DGFP* with UAS-*Luc-RNAi* (control, G), UAS-*hoka-RNAi* 13704R-1 (H) or UAS-*hoka-RNAi hokalR-L* (I) at 10 days after induction, and stained for GFP (green) and DNA (propidium iodide, red). The enhancement of the Jak-Stat pathway activity in the *hoka-RNAi* midgut is shown by the increased expression of the *10xSTAT-DGFP* reporter (H,I). The images (A–I) show the surface views of the midgut. (J) Quantification of PH3⁺ cells. The dot-plots show the numbers of PH3⁺ cells in the individual midguts. Left to right: control *Luc-RNAi* ($n=18$); *hoka-RNAi* 13704R-1 ($n=20$); and *hoka-RNAi hokalR-L* ($n=24$) at 5 days after induction; and control *Luc-RNAi* ($n=23$), *hoka-RNAi* 13704R-1 ($n=21$), *hoka-RNAi hokalR-L* ($n=20$) and *hoka-RNAi hokalR-S* ($n=17$) at 10 days after induction. The bars and numbers in the graph represent the mean PH3⁺ cells in the fly lines. Statistical significance ($P<0.0001$) was evaluated by one-way ANOVA/Tukey's multiple comparisons tests. (K–M) Confocal images of the adult posterior midgut expressing *Myo1A^{ts}-Gal4/UAS-CD8-GFP* with UAS-*Luc-RNAi* (control, K), UAS-*hoka-RNAi* 13704R-1 (L) or UAS-*hoka-RNAi hokalR-L* (M) at 10 days after induction, and stained for CD8-GFP (green), DNA (propidium iodide) (red) and F-actin (blue). The images show longitudinal cross-sections of the midgut. CD8-GFP driven by *Myo1A^{ts}* was expressed in the ECs of each midgut. (N–P'') Confocal images of the adult posterior midgut expressing *Myo1A^{ts}-Gal4/UAS-CD8-GFP* with UAS-*Luc-RNAi* (control, N–N''), UAS-*hoka-RNAi* 13704R-1 (O–O'') or UAS-*hoka-RNAi hokalR-L* (P–P'') at 10 days after induction, and stained for pERM (red in N,N'',O,O'',P,P'') and Dlg (blue in N',N'',O',O'',P',P''). The images show the longitudinal cross-sections of the midgut. CD8-GFP driven by *Myo1A^{ts}* was expressed in the ECs of each midgut. (Q) The diameter of the posterior region of the midgut. The diameter of the midgut was measured just anterior to the Malpighian tubules. Left to right: control *Luc-RNAi* ($n=19$); *hoka-RNAi* 13704R-1 ($n=17$); and *hoka-RNAi hokalR-L* ($n=15$) at 5 days after induction; and control ($n=19$), *hoka-RNAi* 13704R-1 ($n=19$), *hoka-RNAi hokalR-L* ($n=21$) and *hoka-RNAi hokalR-S* ($n=19$) at 10 days after induction. Data are mean \pm s.e.m. Statistical significance ($P<0.0001$) was evaluated using one-way ANOVA/Tukey's multiple comparisons tests. NS, not significant.

induce cell aggregation, which is a criterion for cell adhesion activity (data not shown).

The role of Hoka in sSJ organization

The loss of an sSJ protein results in the mislocalization of other sSJ proteins (Izumi et al., 2012, 2016), indicating that sSJ proteins are mutually dependent for their sSJ localization. In the *ssk*-deficient midgut, Mesh and Tsp2A were distributed diffusely in the cytoplasm (Izumi et al., 2012, 2016). In the *mesh* mutant midgut, Ssk was localized at the apical and lateral membranes, whereas Tsp2A was distributed diffusely in the cytoplasm (Izumi et al., 2012, 2016). In the *Tsp2A*-mutant midgut, Ssk was localized at the apical and lateral membranes, whereas Mesh was distributed diffusely in the cytoplasm (Izumi et al., 2016). Among these three mutants, the mislocalization of Ssk, Mesh or Tsp2A is consistent; Mesh and Tsp2A were distributed in the cytoplasm, whereas Ssk was localized at the apical and lateral membranes. However, in the *hoka*-mutant larval midgut, Mesh and Tsp2A were distributed along the lateral membrane, whereas Ssk was mislocalized to the apical and lateral membranes. Interestingly, in some *hoka* mutant midguts, Ssk, Mesh and Tsp2A were localized to the apicolateral region, as observed in the wild-type midgut. Differences in subcellular

misdistribution of sSJ proteins between the *hoka* mutant and the *ssk*, *mesh* and *Tsp2A*-mutants indicate that the role of Hoka in the process of sSJ formation is different from that of Ssk, Mesh or Tsp2A. Ssk, Mesh and Tsp2A may form the core complex of sSJs, and these proteins are indispensable for the generation of sSJs, whereas Hoka facilitates the arrangement of the primordial sSJs at the correct position, i.e. the apicolateral region. This Hoka function may also be important for rapid paracellular barrier repair during the epithelial cell turnover in the adult midgut. Notably, during the sSJ formation process of OELP, the sSJ targeting property of Hoka was similar to that of Mesh, implying that Hoka may have a close relationship with Mesh, rather than Ssk and Tsp2A during sSJ development.

The role of Hoka in intestinal homeostasis

The knockdown of *hoka* in the adult midgut leads to a shortened lifespan in adult flies, intestinal barrier dysfunction, increased ISC proliferation and the accumulation of ECs. These results are consistent with the recent observation for *ssk*, *mesh* and *Tsp2A-RNAi* in the adult midgut (Salazar et al., 2018; Xu et al., 2019; Izumi et al., 2019; Chen et al., 2020). The intestinal barrier dysfunction caused by RNAi for sSJ proteins may permit the leakage of particular substances from the midgut lumen, which may induce particular cells to secrete cytokines and growth factors for ISC proliferation. Alternatively, sSJs or sSJ-associated proteins may be directly involved in the secretion of cytokines and growth factors through the regulation of intracellular signaling in the ECs. In the latter case, Xu et al. (2019) showed that *Tsp2A* knockdown in ISCs/EBs or ECs hampers the endocytic degradation of aPKC, thereby activating the aPKC and Yki signaling pathways, leading to ISC overproliferation in the midgut. Therefore, Xu et al. (2019) proposed that sSJs are directly involved in the regulation of aPKC and the Hippo pathway-mediated intracellular signaling for ISC proliferation. We have shown that the expression of *hoka-RNAi* together with *aPKC-RNAi* or *yki-RNAi* in ECs significantly reduced ISC overproliferation caused by *hoka-RNAi*. Thus, aPKC- and Yki-mediated ISC overproliferation appears to commonly occur in sSJ protein-deficient midguts. However, the possibility that the leakage of particular substances through the paracellular route may be involved in ISC overproliferation in the sSJ proteins-deficient midgut cannot be excluded.

It has been reported that apical aPKC staining is observed in ISCs but is barely detectable in ECs (Goulas et al., 2012). We found that the expression of *hoka-RNAi* in ECs increased aPKC staining in the midgut. Additionally, in the *hoka-RNAi* midgut, apical aPKC staining was observed in ISCs and in differentiated cells, including EC-like cells. Thus, apical and increased cytoplasmic aPKC may contribute to ISC overproliferation. Interestingly, EC-like cells in the *hoka-RNAi* midgut do not always localize aPKC to the apical regions. Apical aPKC staining was detected in EC-like cells mounted by other cells but was barely detectable in the lumen-facing EC-like cells. These mounted cells are thought to be newly generated cells after the induction of *hoka-RNAi*, which may not be able to exclude aPKC from the apical region in the crowded cellular environment. A recent study showed that aberrant sSJ formation caused by *Tsp2A*-depletion impairs aPKC endocytosis and increases aPKC localization in the membrane of cell borders (Xu et al., 2019). The sSJ proteins, including Hoka, may also regulate endocytosis to exclude aPKC from the apical membrane of ECs. The identification of molecules involved in aPKC-mediated ISC proliferation may provide a better understanding of the aPKC-mediated signaling pathway, as well as the mechanisms underlying

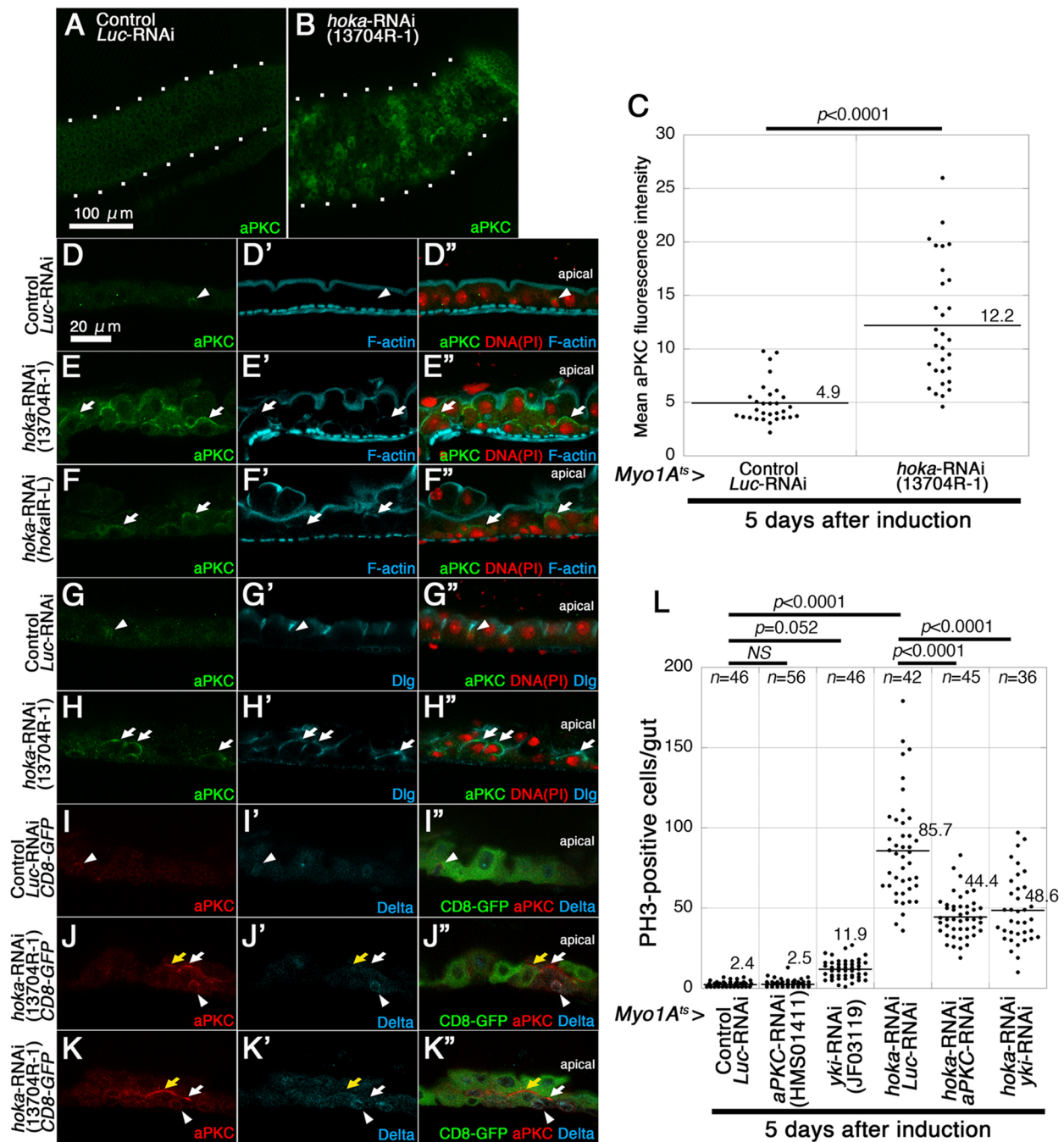


Fig. 8. The depletion of *aPKC* and *yki* from *hoka-RNAi* ECs results in the reduction of ISC overproliferation caused by *hoka-RNAi*. (A,B) Confocal images of the adult posterior midgut expressing *Myo1A^{ts}-Gal4* with UAS-*Luc-RNAi* (control, A) or UAS-*hoka-RNAi* 13704R-1 (B) at 5 days after induction, and stained for *aPKC* (green). The images show the surface views of the midgut. The outline of the midgut is delineated by dots. (C) Dot-plots showing the mean *aPKC* fluorescence intensity in the posterior midgut. The bars and the numbers in the graph display the mean fluorescence intensity of the control (*Luc-RNAi*) or *hoka-RNAi* 13704R-1 midgut. The mean fluorescence intensity was calculated from three random (100 μm \times 100 μm) fields per midgut ($n=10$ for each genotype). (D–H'') Confocal images of the adult posterior midgut expressing *Myo1A^{ts}-Gal4* with UAS-*Luc-RNAi* (control, D–D''), UAS-*hoka-RNAi* 13704R-1 (E–E'', H–H'') or UAS-*hoka-RNAi* *hokalR-L* (F–F'') at 5 days after induction, and stained for *aPKC* (green in D–D'', E–E'', H–H''), F-actin (blue in D'–F', D''–F'') and Dlg (blue in G', G'', H', H''). The arrowheads indicate the cells with apical *aPKC* staining and a small nucleus in the control midgut. The arrows indicate cells with apical *aPKC* staining and a large nucleus in the *hoka-RNAi* midgut. (I–K'') Confocal images of the adult posterior midgut expressing *Myo1A^{ts}-Gal4*/UAS-*CD8-GFP* with UAS-*Luc-RNAi* (control, I–I'') or UAS-*hoka-RNAi* 13704R-1 (J–J'') at 5 days after induction, and stained for *aPKC* (red in I', J', K', K'') and Delta (blue in I'', J'', K'', K''). The arrowheads indicate Delta and *aPKC* double-positive cells. The white and yellow arrows indicate the apical *aPKC*⁺ and *CD8-GFP*[−] cells, and the apical *aPKC* and *CD8-GFP*-double positive cells, respectively. *CD8-GFP* driven by *Myo1A^{ts}* was expressed in the ECs of each midgut. The images (D–K'') show the longitudinal cross-sections of the midgut. (L) Quantification of PH3⁺ cells. The dot-plots show the numbers of PH3⁺ cells in the individual midguts. Left to right: Control *Luc-RNAi* ($n=46$); *aPKC-RNAi* HMS01411 ($n=56$); *yki-RNAi* JF03119 ($n=46$); *hoka-RNAi* 13704R-1 together with *Luc-RNAi* ($n=42$); *hoka-RNAi* 13704R-1 together with *aPKC-RNAi* HMS01411 ($n=45$); and *hoka-RNAi* 13704R-1 together with *yki-RNAi* JF03119 ($n=36$) at 5 days after induction. Bars and numbers in the graph represent the mean PH3⁺ cells in the fly lines. Statistical significance ($p<0.001$ in C and $p<0.0001$ in L) was evaluated by Mann–Whitney *U*-test (C) and one-way ANOVA/Tukey's multiple comparisons tests (L). NS, not significant.

the increased expression and apical targeting of aPKC in the ECs deficient for sSJ proteins.

MATERIALS AND METHODS

Fly stocks and genetics

Fly stocks were reared on a standard cornmeal fly medium at 25°C. *w¹¹¹⁸* flies were used as wild-type flies unless otherwise specified. The other fly stocks used were *w*, *da-GAL4/TM6B*, *Tb* [#55851; Bloomington *Drosophila* Stock Center (BDSC), Bloomington, IN, USA], *y w*; *Myo1A-GAL4* [#112001; *Drosophila* Genetic Resource Center (DGRC), Kyoto, Japan], *tubP-GAL80^{ts}* (#7019; BDSC), *y w*; *Pin^Y/CyO*; *UAS-mCD8-GFP* (#5130; BDSC), *w*; *10xStat92E-DGFP/TM6C Sb Tb* (#26200; BDSC), *y w*; *esg-lacZ/CyO* (#108851; DGRC) and *FRT19A*; *ry* (#106464; DGRC). The RNAi lines used were *hoka*-RNAi [#13704R-1, NIG-Fly, Mishima, Japan], *Luciferase (Luc)*-RNAi (#31603; BDSC), *aPKC*-RNAi (HMS01411, #35001; BDSC) and *yki*-RNAi (JF03119, #31965; BDSC). The mutant stocks used were *Df(3L)ssk* (Yanagihashi et al., 2012), *mesh^{l04955}* (#18826; BDSC) (Izumi et al., 2012) and *Tsp2A¹⁻²* (Izumi et al., 2016). For the phenotype rescue experiment, pUAST vectors (Brand and Perrimon, 1993) containing *hoka*-GFP were constructed, and a fly strain carrying this construct was established. The stocks used for the generation of *hoka* mutants were *y² cho² v¹* (TBX-0004), *y¹ v¹ P{nos-phiC31/int.NLS}X*; attP40 (II) (TBX-0002; NIG-Fly), *y² cho² v¹*; *Sco/CyO* (TBX-0007; NIG-Fly), *y² cho² v¹ P{nosP-Cas9, y⁺, v⁺}1A/FM7c, KrGAL4 UAS-GFP* (CAS0002; NIG-Fly) and *y² cho² v¹*; *PrDr/TM6C, Sb Tb* (TBX-0010; NIG-Fly).

Antibodies

The following custom antibodies were used: rabbit anti-Hoka (29-1, 1:2000; 29-2, 1:2000; see below for details of production); rabbit anti-Mesh (955-1; 1:1000), rabbit anti-Mesh (995-1; 1:1000) and rat anti-Mesh (8002; 1:500) (previously described by Izumi et al., 2012); rabbit anti-Ssk (6981-1; 1:1000; previously described by Yanagihashi et al., 2012); and rabbit anti-Tsp2A (302AP, 1:200; previously described by Izumi et al., 2016). The following commercial antibodies were used: mouse anti-Dlg [4F3, Developmental Studies Hybridoma Bank (DSHB); 1:50]; mouse anti-Delta (C594.9B; DSHB; 1:20); rabbit anti-PH3 (06-570; Millipore, Darmstadt, Germany; 1:1000); rabbit anti-dpERK (4370; Cell Signaling Technology, Danvers, MA; 1:500); rabbit anti-phospho-Ezrin/Radixin/Moesin (pERM; 3726; Cell Signaling Technology; 1:200); rat anti-GFP (GF090R; Nacalai Tesque; 1:1000); rabbit anti-GFP (598; MBL, Nagoya, Japan; 1:1000); and rabbit anti-aPKC (sc-216; Santa Cruz, Dallas, TX, USA; 1:500). Alexa Fluor 488-conjugated (A21206; Invitrogen), and Cy3- and Cy5-conjugated (712-165-153 and 715-175-151, Jackson ImmunoResearch Laboratories, West Grove, PA, USA) secondary antibodies were used at 1:400. Actin was stained with Alexa Fluor 568 phalloidin (A12380; Thermo Fisher; 1:1000) or Alexa Fluor 647 phalloidin (A22287; Thermo Fisher; 1:1000). Nuclei were stained with propidium iodide (Nacalai Tesque; 0.1 mg/ml).

Deficiency screen

Embryos of deficiency lines were obtained from the BDSC and the DGRC. The deficiency screen was performed as described previously (Izumi et al., 2016).

cDNA cloning and expression vector construction

The open reading frame (ORF) of *hoka*, including the initiation codon, was amplified by PCR with the forward primer harboring an EcoRI site (5'-cgggaattcACGAAAACGACGGAAATGAAGTTGGCT-3') and the reverse primer having a BglII site (5'-gaagatctGTGACAATAGCGGTGG-CATGCG-3'), and the EcoRI and BglII sites containing *Drosophila* embryonic cDNA were cloned into the EcoRI and BglII sites of the pUAST vector (Brand and Perrimon, 1993). To generate an expression vector for the C-terminal EGFP-tagged Hoka, EGFP cDNA with 3' and 5' XhoI sites was cloned into the XhoI site of pUAST-*hoka*. To generate RNAi lines (*hoka*IR-L and *hoka*IR-S), a DNA fragment containing 1 to 682 (*hoka*IR-L) or 160 to 682 (*hoka*IR-S) of the *hoka* ORF was amplified by PCR with the forward primer harboring an EcoRI site (*hoka*IR-L, 5'-cgggaattcATGAAGTTGGCTAAGA-AGTGC-3'; *hoka*IR-S, 5'-cgggaattcATCGTTTGTGTAGCGGTAGGT-3') or a XhoI site (*hoka*IR-L, 5'-ccgctcgagATGAAGTT-GGCTAAGAAGTG-3';

*hoka*IR-S, 5'-ccgctcgagATCGTTTGTGTAGCGGTAGGT-3'), and the reverse primer having a BglII site (5'-gaagatctCAGACAATAGCGGTGG-CATG-3'). The two types of DNA fragments were inserted into pUAST as a head-to-head dimer and transformed into SURE2 competent cells (200152; Agilent Technologies, Santa Clara, CA, USA). Transgenic flies were generated by standard P-element transformation procedures.

Generation of Tsp2A mutants

Generation of *hoka* mutants using the CRISPR/Cas9 system was performed according to the method described by Kondo and Ueda (2013). To construct a guide RNA (gRNA) expression vector for *hoka*, two complementary 24 bp oligonucleotides of the target sequence with 4 bp overhangs on both ends (5'-cttcGGCCTGCTGCCTGCAAGAAT-3' and 5'-aacATTCTTG-CAGGCAGCAGGCC-3') were annealed to generate a double-stranded DNA fragment that was cloned into BbsI-digested pBFv-U6.2 (NIG-Fly) (pBFv-U6.2-*hoka*CR1). pBFv-U6.2-*hoka*CR1 was injected into the *y¹ v¹ nos-phiC31*; attP40 host (Bischof et al., 2007). Surviving G₀ males were individually crossed to *y² cho² v¹* virgins. A single male transformant from each cross was mated to *y² cho² v¹*; *Sco/CyO* virgins. Offspring in which the transgene was balanced were collected to establish a stock. Males carrying a U6.2-*hoka*CR1 transgene were crossed to *nos*-Cas9 females (*y² cho² v¹ P{nosP-Cas9, y⁺, v⁺}1A*) to obtain founder flies that have both the U6.2-*hoka*CR1 and the *nos*-Cas9 transgenes. Male founders were crossed to *y² cho² v¹*; *PrDr/TM6C, Sb Tb* female flies. Each male possessing *y² cho² v¹*/Y; +/TM6C, *Sb Tb* genotype was crossed to *y² cho² v¹*; *PrDr/TM6C, Sb Tb* female flies and the offspring possessing the *y² cho² v¹*; +/TM6C, *Sb Tb* genotype were collected to establish the lines. The embryos of the lethal lines were immunostained for Hoka. Genomic DNA of the *hoka⁻* lines was extracted and analyzed for mutations in the *hoka* gene locus.

Production of polyclonal antibodies against Hoka

The amino acids 77-136 encoding the cytoplasmic region of the Hoka protein were cloned into pGEX-6P (GE Healthcare) to produce a Glutathione S-transferase fusion protein. The proteins were expressed in *Escherichia coli* (DH5α) and purified using Glutathione Sepharose 4B (GE Healthcare). Polyclonal antibodies were generated in rabbits [29-1 and 29-2 by Kiwa Laboratory Animals (Wakayama, Japan)].

Immunostaining

Embryos were fixed with 3.7% formaldehyde in PBS for 20 min. Adult flies and larvae were dissected in Hanks' Balanced Salt Solution and the midgut was fixed with 4% paraformaldehyde in PBS/0.2% Tween 20 for 30 min. The fixed specimens were washed three times with PBS/0.4% Triton X-100 and were blocked with 5% skimmed milk in PBS/0.2% Tween 20. Thereafter, the samples were incubated with primary antibodies at 4°C overnight, washed three times with PBS/0.2% Tween 20, and incubated with secondary antibodies for 3 h. After another three washes, the samples were mounted in Fluoro-KEEPER antifade reagent (12593-64; Nacalai Tesque, Kyoto, Japan). Images were acquired using a confocal microscope (Model TCS SPE; Leica Microsystems, Wetzlar, Germany) and its accompanying software and the HC PLAN Apochromat 20× NA 0.7 and HCX PL objective lenses (Leica Microsystems). Images were processed with Adobe Photoshop software.

Electron microscopy

First-instar larvae of wild-type or *hoka^{x2/1}* mutants were dissected and fixed overnight at 4°C with a mixture of 2.5% glutaraldehyde and 2% paraformaldehyde in 0.1 M cacodylate buffer (pH 7.4). The specimens including the midguts were prepared as described previously (Izumi et al., 2012). Ultrathin sections (50–100 nm) were stained doubly with 4% hafnium (IV) chloride and lead citrate, and observed using a JEM-1010 electron microscope (JEOL, Tokyo, Japan) equipped with a Veleta TEM CCD Camera (Olympus, Tokyo, Japan) at an accelerating voltage of 80 kV.

Co-immunoprecipitation and western blotting

Fly wild-type embryos and embryos expressing EGFP-Tsp2A or GFP (*da-Gal4*>UAS-EGFP-Tsp2A or UAS-GFP) were mixed with a fivefold

volume of lysis buffer [30 mM Tris-HCl (pH 7.5), 150 mM NaCl and 1% Brij97 (P6136, Sigma-Aldrich, St Louis, MO, USA)] and protease inhibitor cocktail (25955-11, Nacalai Tesque, Kyoto, Japan), and homogenized using a pestle for 1.5 ml microfuge tubes. The method for immunoprecipitation was essentially the same as described previously (Izumi et al., 2016). Rabbit anti-Hoka (29-1, 29-2), rabbit anti-Mesh (995-1), rabbit anti-Ssk (6981-1) and rabbit anti-GFP (598, MBL, Nagoya, Japan) antibodies were used for immunoprecipitation. Immunocomplexes and extracts of the first-instar larva were separated on SDS-polyacrylamide gels, transferred to polyvinylidene difluoride membranes and western blot analyses were performed using rabbit anti-Hoka (29-1; 1:2000, 29-2; 1:2000), rabbit anti-Mesh (995-1; 1:1000), rabbit anti-Ssk (6981-1; 1:1000), rabbit anti-GFP (598; 1:1000, MBL, Nagoya, Japan) and mouse anti- α -tubulin (DM-1A; 1:1000, Sigma-Aldrich) antibodies. The molecular weights of protein bands were estimated using the Precision Plus Protein Dual Color Standards (#161-0374; Bio-Rad, Hercules, CA, USA).

Conditional expression of UAS transgenes (TARGET system)

Flies were crossed and grown at 18°C until eclosion. Adult female flies were collected 2–5 days after eclosion and transferred to 29°C for the inactivation of Gal80.

Barrier integrity (Smurf) assay

Flies at 2–5 days of age were placed in empty vials containing a piece of paper soaked in 2.5% (w/v) Blue Dye No. 1 (Tokyo Chemical Industry, Tokyo, Japan)/5% sucrose solution at 50–60 flies/vial. After 2 days at 18°C, the flies were placed in new vials containing paper soaked in Blue Dye/sucrose and transferred to 29°C. Loss of midgut barrier function was determined when the dye was observed outside the gut (Rera et al., 2011, 2012). Flies were transferred to new vials every 2 days.

Quantification of aPKC intensity

To measure the fluorescence intensity of aPKC, a z-projection was created from the R5 region of the posterior midgut. The projection included stacks of the EC layer of the midgut. The mean gray value of the green channel was collected from three random (100 μ m \times 100 μ m) fields per midgut using ImageJ software 1.52k (National Institutes of Health, Bethesda, MD, USA) and we subtracted the background values measured from the outside area surrounding the midgut.

Statistical analyses

Statistical significance was evaluated using the Mann–Whitney *U*-test, Student's *t*-test and one-way ANOVA/Tukey's multiple comparisons test (KaleidaGraph software; Synergy Software, Reading, PA, USA). Values of $P < 0.05$ were considered significant.

Acknowledgements

We thank M. Motoishi for technical assistance and all members of the Furuse laboratory for helpful discussions. We thank the BDSC, DGRC at the Kyoto Institute of Technology, and NIG-Fly for fly stocks. We would like to thank Editage (www.editage.com) for their assistance with English language editing.

Competing interests

The authors declare no competing or financial interests.

Author contributions

Conceptualization: Y.I., K.F.; Resources: Y.I.; Data curation: Y.I.; Writing - original draft: Y.I.; Writing - review & editing: Y.I., M.F.; Visualization: Y.I., K.F.; Supervision: M.F.; Project administration: Y.I.; Funding acquisition: Y.I., M.F.

Funding

This work was supported by a Grant-in-Aid for Scientific Research (C) (15K07048 and 19K06650) to Y.I. from the Japan Society for the Promotion of Science, and by the Funding Program for Next Generation, World Leading Researchers (NEXT Program) from the Japan Society for the Promotion of Science initiated by the Council for Science and Technology Policy (LS084) to M.F.

Supplementary information

Supplementary information available online at <https://jcs.biologists.org/lookup/doi/10.1242/jcs.257022.supplemental>

Peer review history

The peer review history is available online at <https://jcs.biologists.org/lookup/doi/10.1242/jcs.257022.reviewer-comments.pdf>

References

- Banerjee, S., Sousa, A. D. and Bhat, M. A. (2006). Organization and function of septate junctions: an evolutionary perspective. *Cell Biochem. Biophys.* **46**, 65–78. doi:10.1385/CBB:46:1:65
- Beebe, K., Lee, W. C. and Micchelli, C. A. (2010). JAK/STAT signaling coordinates stem cell proliferation and multilineage differentiation in the Drosophila intestinal stem cell lineage. *Dev. Biol.* **338**, 28–37. doi:10.1016/j.ydbio.2009.10.045
- Beyenbach, K. W., Schone, F., Breitsprecher, L. F., Tiburcy, F., Furuse, M., Izumi, Y., Meyer, H., Jonusaite, S., Rodan, A. R. and Paululat, A. (2020). The septate junction protein Tetraspanin 2A is critical to the structure and function of Malpighian tubules in Drosophila melanogaster. *Am. J. Physiol. Cell Physiol.* **318**, C1107–C1122. doi:10.1152/ajpcell.00061.2020
- Bischof, J., Maeda, R. K., Hediger, M., Karch, F. and Basler, K. (2007). An optimized transgenesis system for Drosophila using germ-line-specific phiC31 integrases. *Proc. Natl. Acad. Sci. USA* **104**, 3312–3317. doi:10.1073/pnas.0611511104
- Biteau, B. and Jasper, H. (2011). EGF signaling regulates the proliferation of intestinal stem cells in Drosophila. *Development* **138**, 1045–1055. doi:10.1242/dev.056671
- Brand, A. H. and Perrimon, N. (1993). Targeted gene expression as a means of altering cell fates and generating dominant phenotypes. *Development* **118**, 401–415.
- Buchon, N., Broderick, N. A., Kuraishi, T. and Lemaitre, B. (2010). Drosophila EGFR pathway coordinates stem cell proliferation and gut remodeling following infection. *BMC Biol.* **8**, 152. doi:10.1186/1741-7007-8-152
- Chen, J., Sayadian, A. C., Lowe, N., Lovegrove, H. E. and St Johnston, D. (2018). An alternative mode of epithelial polarity in the Drosophila midgut. *PLoS Biol.* **16**, e3000041. doi:10.1371/journal.pbio.3000041
- Chen, H. J., Li, Q., Nirala, N. K. and Ip, Y. T. (2020). The snakeskin-mesh complex of smooth septate junction restricts yorkie to regulate intestinal homeostasis in Drosophila. *Stem Cell Reports* **14**, 828–844. doi:10.1016/j.stemcr.2020.03.021
- Furuse, M. and Izumi, Y. (2017). Molecular dissection of smooth septate junctions: understanding their roles in arthropod physiology. *Ann. N. Y. Acad. Sci.* **1397**, 17–24. doi:10.1111/nyas.13366
- Furuse, M. and Tsukita, S. (2006). Claudins in occluding junctions of humans and flies. *Trends Cell Biol.* **16**, 181–188. doi:10.1016/j.tcb.2006.02.006
- Gabay, L., Seger, R. and Shilo, B. Z. (1997). MAP kinase in situ activation atlas during Drosophila embryogenesis. *Development* **124**, 3535–3541.
- Goulas, S., Conder, R. and Knoblich, J. A. (2012). The Par complex and integrins direct asymmetric cell division in adult intestinal stem cells. *Cell Stem Cell* **11**, 529–540. doi:10.1016/j.stem.2012.06.017
- Green, C. R. and Bergquist, P. R. (1982). Phylogenetic-relationships within the invertebrata in relation to the structure of septate junctions and the development of occluding junctional types. *J. Cell Sci.* **53**, 279–305.
- Guo, Z. and Ohlstein, B. (2015). Stem cell regulation. Bidirectional Notch signaling regulates Drosophila intestinal stem cell multipotency. *Science* **350**, aab0988. doi:10.1126/science.aab0988
- Izumi, Y. and Furuse, M. (2014). Molecular organization and function of invertebrate occluding junctions. *Semin. Cell Dev. Biol.* **36**, 186–193. doi:10.1016/j.semdb.2014.09.009
- Izumi, Y., Yanagihashi, Y. and Furuse, M. (2012). A novel protein complex, Mesh-Ssk, is required for septate junction formation in the Drosophila midgut. *J. Cell Sci.* **125**, 4923–4933. doi:10.1242/jcs.112243
- Izumi, Y., Motoishi, M., Furuse, K. and Furuse, M. (2016). A tetraspanin regulates septate junction formation in Drosophila midgut. *J. Cell Sci.* **129**, 1155–1164. doi:10.1242/jcs.180448
- Izumi, Y., Furuse, K. and Furuse, M. (2019). Septate junctions regulate gut homeostasis through regulation of stem cell proliferation and enterocyte behavior in Drosophila. *J. Cell Sci.* **132**, jcs232108. doi:10.1242/jcs.232108
- Jiang, H., Patel, P. H., Kohlmaier, A., Grenley, M. O., McEwen, D. G. and Edgar, B. A. (2009). Cytokine/Jak/Stat signaling mediates regeneration and homeostasis in the Drosophila midgut. *Cell* **137**, 1343–1355. doi:10.1016/j.cell.2009.05.014
- Jiang, H., Grenley, M. O., Bravo, M. J., Blumhagen, R. Z. and Edgar, B. A. (2011). EGFR/Ras/MAPK signaling mediates adult midgut epithelial homeostasis and regeneration in Drosophila. *Cell Stem Cell* **8**, 84–95. doi:10.1016/j.stem.2010.11.026
- Jiang, H., Tian, A. and Jiang, J. (2016). Intestinal stem cell response to injury: lessons from Drosophila. *Cell. Mol. Life Sci.* **73**, 3337–3349. doi:10.1007/s00018-016-2235-9
- Jonusaite, S., Donini, A. and Kelly, S. P. (2016). Occluding junctions of invertebrate epithelia. *J. Comp. Physiol. B* **186**, 17–43. doi:10.1007/s00360-015-0937-1
- Jonusaite, S., Beyenbach, K. W., Meyer, H., Paululat, A., Izumi, Y., Furuse, M. and Rodan, A. R. (2020). The septate junction protein Mesh is required for epithelial morphogenesis, ion transport, and paracellular permeability in the

- Drosophila Malpighian tubule. *Am. J. Physiol. Cell Physiol.* **318**, C675-C694. doi:10.1152/ajpcell.00492.2019
- Karpowicz, P., Perez, J. and Perrimon, N.** (2010). The Hippo tumor suppressor pathway regulates intestinal stem cell regeneration. *Development* **137**, 4135-4145. doi:10.1242/dev.060483
- Kondo, S. and Ueda, R.** (2013). Highly improved gene targeting by germline-specific Cas9 expression in Drosophila. *Genetics* **195**, 715-721. doi:10.1534/genetics.113.156737
- Lane, N. J. and Swales, L. S.** (1982). Stages in the assembly of pleated and smooth septate junctions in developing insect embryos. *J. Cell Sci.* **56**, 245-262.
- Lane, N. J., Dallai, R., Martinucci, G. and Burighel, P.** (1994). Electron microscopic structure and evolution of epithelial junctions. In *Molecular Mechanisms of Epithelial Cell Junctions: From Development to Disease* (ed. S. Citi), pp. 23-43. Austin, TX: RG Landes Co.
- Mcguire, S. E., Mao, Z. and Davis, R. L.** (2004). Spatiotemporal gene expression targeting with the TARGET and gene-switch systems in Drosophila. *Sci. STKE* **2004**, pl6. doi:10.1126/stke.2202004pl6
- Micchelli, C. A. and Perrimon, N.** (2006). Evidence that stem cells reside in the adult Drosophila midgut epithelium. *Nature* **439**, 475-479. doi:10.1038/nature04371
- Ohlstein, B. and Spradling, A.** (2006). The adult Drosophila posterior midgut is maintained by pluripotent stem cells. *Nature* **439**, 470-474. doi:10.1038/nature04333
- Ohno, S., Goulas, S. and Hirose, T.** (2015). *Cell Polarity 1: The PAR3-aPKC-PAR6 Complex* (ed. K. Ebneth), pp. 3-23. Switzerland: Springer International Publishing.
- Osman, D., Buchon, N., Chakrabarti, S., Huang, Y. T., Su, W. C., Poidevin, M., Tsai, Y. C. and Lemaitre, B.** (2012). Autocrine and paracrine unpaired signaling regulate intestinal stem cell maintenance and division. *J. Cell Sci.* **125**, 5944-5949. doi:10.1242/jcs.113100
- Ren, F., Wang, B., Yue, T., Yun, E.-Y., Ip, Y. T. and Jiang, J.** (2010). Hippo signaling regulates Drosophila intestine stem cell proliferation through multiple pathways. *Proc. Natl. Acad. Sci. USA* **107**, 21064-21069. doi:10.1073/pnas.1012759107
- Rera, M., Bahadorani, S., Cho, J., Koehler, C. L., Ulgherait, M., Hur, J. H., Ansari, W. S., Lo, T., Jr, Jones, D. L. and Walker, D. W.** (2011). Modulation of longevity and tissue homeostasis by the Drosophila PGC-1 homolog. *Cell Metab.* **14**, 623-634. doi:10.1016/j.cmet.2011.09.013
- Rera, M., Clark, R. I. and Walker, D. W.** (2012). Intestinal barrier dysfunction links metabolic and inflammatory markers of aging to death in Drosophila. *Proc. Natl. Acad. Sci. USA* **109**, 21528-21533. doi:10.1073/pnas.1215849110
- Resnik-Docampo, M., Koehler, C. L., Clark, R. I., Schinaman, J. M., Sauer, V., Wong, D. M., Lewis, S., D'alterio, C., Walker, D. W. and Jones, D. L.** (2017). Tricellular junctions regulate intestinal stem cell behaviour to maintain homeostasis. *Nat. Cell Biol.* **19**, 52-59. doi:10.1038/ncb3454
- Rouka, E., Gourgoulis, N., Lupold, S., Hatzoglou, C., Gourgoulis, K., Blanckenhorn, W. U. and Zargiannis, S. G.** (2020). The Drosophila septate junctions beyond barrier function: Review of the literature, prediction of human orthologs of the SJ-related proteins and identification of protein domain families. *Acta Physiol. (Oxf.)* **231**, e13527. doi:10.1111/apha.13527
- Salazar, A. M., Resnik-Docampo, M., Ulgherait, M., Clark, R. I., Shirasu-Hiza, M., Jones, D. L. and Walker, D. W.** (2018). Intestinal snakeskin limits microbial dysbiosis during aging and promotes longevity. *iScience* **9**, 229-243. doi:10.1016/j.isci.2018.10.022
- Shaw, R. L., Kohlmaier, A., Polesello, C., Veelken, C., Edgar, B. A. and Tapon, N.** (2010). The Hippo pathway regulates intestinal stem cell proliferation during Drosophila adult midgut regeneration. *Development* **137**, 4147-4158. doi:10.1242/dev.052506
- Tepass, U. and Hartenstein, V.** (1994). The development of cellular junctions in the *Drosophila* embryo. *Dev. Biol.* **161**, 563-596. doi:10.1006/dbio.1994.1054
- Tepass, U., Tanentzapf, G., Ward, R. and Fehon, R.** (2001). Epithelial cell polarity and cell junctions in Drosophila. *Annu. Rev. Genet.* **35**, 747-784. doi:10.1146/annurev.genet.35.102401.091415
- Wu, V. M. and Beitel, G. J.** (2004). A junctional problem of apical proportions: epithelial tube-size control by septate junctions in the Drosophila tracheal system. *Curr. Opin. Cell Biol.* **16**, 493-499. doi:10.1016/j.ceb.2004.07.008
- Xu, C., Tang, H. W., Hung, R. J., Hu, Y., Ni, X., Housden, B. E. and Perrimon, N.** (2019). The septate junction protein Tsp2A restricts intestinal stem cell activity via endocytic regulation of aPKC and hippo signaling. *Cell Rep* **26**, 670-688.e676. doi:10.1016/j.celrep.2018.12.079
- Yanagihashi, Y., Usui, T., Izumi, Y., Yonemura, S., Sumida, M., Tsukita, S., Uemura, T. and Furuse, M.** (2012). Snakeskin, a membrane protein associated with smooth septate junctions, is required for intestinal barrier function in Drosophila. *J. Cell Sci.* **125**, 1980-1990. doi:10.1242/jcs.096800
- Zheng, Y. and Pan, D.** (2019). The hippo signaling pathway in development and disease. *Dev. Cell* **50**, 264-282. doi:10.1016/j.devcel.2019.06.003
- Zhou, F., Rasmussen, A., Lee, S. and Agaisse, H.** (2013). The UPD3 cytokine couples environmental challenge and intestinal stem cell division through modulation of JAK/STAT signaling in the stem cell microenvironment. *Dev. Biol.* **373**, 383-393. doi:10.1016/j.ydbio.2012.10.023